Trade, Trees, and Lives*

Xinming Du

Lei Li

Eric Zou

June 2025

Abstract

This paper shows a cascading mechanism through which international trade-induced deforestation results in a decline of health outcomes in cities distant from where trade activities occur. We examine Brazil, which has ramped up agricultural export over the last two decades to meet rising global demand. Using a shift-share research design, we first show that export shocks cause substantial local agricultural expansion and a virtual one-for-one decline in forest cover. We then construct a dynamic area-of-effect model that predicts where atmospheric changes should be felt – due to loss of forests that would otherwise serve to filter out and absorb air pollutants as they travel – downwind of the deforestation areas. Leveraging quasi-random variation in these atmospheric connections, we establish a causal link between deforestation upstream and subsequent rises in air pollution and premature deaths downstream, with the mortality effects predominantly driven by cardiovascular and respiratory causes. Our estimates reveal a large telecoupled health externality of trade deforestation: over 700,000 premature deaths in Brazil over the past two decades. This equates to $0.18 loss in statistical life value per $1 agricultural exports over the study period.

Keywords: trade, deforestation, health

JEL Codes: F18, O13, Q23, Q53

* Du: Department of Economics, National University of Singapore (email: xdu@nus.edu.sg); Li: Faculty of Business and Economics and Faculty of Humanities, University of Göttingen (email: lei.li@uni-goettingen.de); Zou: Ross School of Business, University of Michigan and NBER (email: ericzou@umich.edu). We thank Philipp Ager, David Autor, Ricardo Dahis, David Dorn, Rafael Dix-Carneido, Thiemo Fetzer, Lisandra Flach, Bård Harstad, Guojun He, Karen Helene Ulltveit-Moeandre, Andreas Moxnes, Uta Schönberg, Jan Schymik, Arthur Seibold, Joseph Shapiro, Shinsuke Tanaka, Camille Urvoy, Andreas Kotsadam, Ulrich Wagner, Kathrine von Graevenitz, and participants at various seminars for helpful comments. Zihao Chen, Guilherme Lindenmeyer, and Raphaël Pérot provided excellent research assistance. Support by the Deutsche Forschungsgemeinschaft (DFG, German Research Foundation) through CRC TR 224 (Project B06) is gratefully acknowledged. All errors are our own.

1. Introduction

Globalization creates complex interactions between consumption, production, and environmental impacts that occur in locations far apart.[1] This paper demonstrates the importance of such telecoupling for understanding the health burden of international trade. We study Brazil, where agricultural exports have quadrupled in value over the last two decades due to rising global demand. This export boom has been accompanied by substantial forest loss as land is cleared to accommodate the expanding agricultural production. We show that export-driven deforestation in Brazil has far-reaching public health consequences, as the lost forests would otherwise have acted as natural air filters – capturing airborne particulates and absorbing harmful gases – thereby protecting air quality in cities hundreds or even thousands of miles downwind. As a result, trade-induced forest loss in one region can degrade air quality in distant communities. We find that the magnitude of the health effects is substantial, even when compared against the enormous economic value of Brazil's agricultural trade over the study period.

We are motivated by an emerging debate on the "non-economic" effects of trade, particularly with regard to its interaction with the environment (Copeland, Shapiro, and Taylor, 2022). This is especially relevant in developing country context, where the reliance on exporting resource-intensive products plays a key role in achieving development goals (Frank and Schlenker, 2016). In current literature, the environmental costs of deforestation are predominantly associated with climate change and ecosystem disruptions (Copeland, Shapiro, and Taylor, 2022; Balboni et al., 2023). These include projected alterations in global temperature and precipitation patterns (Bonan, 2008), impacts on biodiversity (Dasgupta, 2021), and increased risk of crossing ecosystems tipping point (Franklin and Pindyck, 2018). While such long-run effects are expected to be profoundly important, they are difficult to empirically pin down due to their diffuse and delayed nature. In contrast, our study examines an immediate environmental channel—air pollution—and its direct impact on human health, which can be observed in current

[1] Economists have extensively studied how trade enhances growth (Grossman and Helpman, 1990) and productivity (Alcalá and Ciccone, 2004), and how it interacts with institutional quality (Levchenko, 2007). Empirical studies show international trade could affect the environment in positive or negative ways (e.g., Antweiler et al., 2001; Frankel and Rose, 2005; Managi et al., 2009; Abman and Lundberg, 2020), and emphasize the large spatial ranges of these impacts. Incorporating multiple locations and environmental consequences is important in assessing the overall welfare effects of globalization.

data. The main message is that the environmental costs of trade-induced deforestation are considerable, even when focusing only on short-term cardio-respiratory health impacts.

We begin by estimating the causal effect of agricultural exports on local forest land coverage. During the two decades of our study period (1997–2019), Brazil significantly expanded its agricultural land use, coinciding with a substantial decline in forest cover. This pattern of deforestation is widely suspected to be associated with growing agricultural export demands, particularly from China and the European Union, which drive farmers to employ slash-and-burn methods for rapid land clearing to boost agricultural production. We estimate the causal link between agricultural exports and deforestation using a shift-share research design, which exploits variation in regions' exposure to global demand shocks ("shift") due to historical differences in export capacity across product categories ("share"). Brazilian regions are exposed to idiosyncratic import shocks across a wide range of product categories, providing an apt context for applying the shift-share research design (e.g., Adao, Kolesár, and Morales, 2019; Borusyak, Hull, and Jaravel, 2022). Our estimates show that each 1,000 BRL increase in export per capita reduces forest cover in the area by 0.174 percentage points. Using the same framework, we also demonstrate that areas losing forest simultaneously experience agricultural expansion, primarily in land-intensive crops long associated with deforestation (notably soybeans and sugar).

Next, we estimate the impact of forest loss on downstream environmental and health outcomes. To accomplish this, we need to identify the extent of cross-boundary pollution spillover: the impact of a pollution source—or in our case, the absence of forests that would have reduced pollution—does not conform to administrative boundaries and can extend far beyond its origin (e.g., Heo, Ito, and Kotamarthi, 2023). We develop a simple area-of-effect (AoE) model that predicts the geo-temporal influence of a given city's forest loss by simulating how wind carries air pollutants across space and time. This model yields a comprehensive matrix of "upwind-downwind" linkages that quantify the intensity of pollution transport between each pair of cities in each month. Our model is parsimonious enough to be computationally feasible, yet it captures atmospheric transport realistically: we show that when the model predicts a strong downwind connection between two cities, the measured pollution levels in those cities (which are data that we did *not* use in training the model) are highly correlated; conversely, when the model predicts no connection, the two cities' pollution levels show little co-movement. Put

differently, the AoE model accurately maps potential pollution spillovers across distant locations, allowing us to trace pollution from deforestation areas to downwind populations.[2]

Building on this pollution transport model, we implement a quasi-experimental design to estimate the causal impact of upstream forest loss on downstream outcomes. For each potential "sender" city (a deforestation location) and "receiver" city (downwind of that sender), we relate changes in the sender's forest cover to the receiver's pollution and health outcomes, allowing the strength of this relationship to vary with the predicted downwind linkage intensity from the AoE model. The regressions include high-dimensional fixed effects (such as sender–receiver pair by month-of-year fixed effects and year fixed effects) to exploit quasi-random variation in wind patterns, thereby isolating how upwind deforestation influences downwind conditions.

Our findings show that deforestation in upwind cities significantly leads to increased air pollution and higher mortality rates in downwind cities. The mortality effect is primarily driven by excess deaths from cardiovascular and respiratory causes, consistent with a pollution exposure pathway. Falsification tests show that deforestation had no effect on health outcomes that are plausibly unrelated to air quality (e.g. accidental death rates), and periods with minimal wind connectivity between a given city pair exhibit no pollution or mortality impact.

Losses in upwind forests can affect downwind air quality through two main pathways. The first is the loss of natural filtration: deforestation eliminates the forest's capacity to filter and absorb airborne pollutants, allowing more pollution to reach downwind areas. The second is a fire effect, as deforestation (often via slash-and-burn) increases the frequency of wildfires that produce smoke drifting into downwind cities. To disentangle these channels, we incorporate satellite data on fire activity into our analysis. We show that when we control flexibly for upwind fire emissions, our pollution and mortality estimates remain virtually unchanged. This indicates that the bulk of the downwind impact is attributable to lost pollution filtration by forests, with the fire pathway playing only a minor role in our context.

[2] An expanding body of literature has leveraged variability in wind conditions to estimate the causal effects of air pollution (e.g., Deryugina et al., 2019; Rangel and Vogl, 2019; Anderson, 2020; Graff Zivin et al., 2023; Guidetti, Pereda, and Severnini, 2024). A key methodological innovation in our work is the development of a computationally feasible approach to build a comprehensive matrix of wind transport relationships across city pairs. This is crucial when the researcher's goal is not only to measure the burden of pollution in the destination area but also to trace that burden back to its sources.

Together, our estimates can be integrated to gauge the overall impact of trade-induced deforestation. We calculate that Brazil's agricultural export growth over 1997–2019 was responsible for approximately 3.6 million hectares of forest loss, which in turn caused an estimated 732,000 excess premature deaths across Brazil via increased pollution. In monetary terms, the lost life years correspond to roughly 513 billion USD in life value loss using standard Value of Statistical Life (VSL) estimates, equivalent to about 18% of the total agricultural export value of Brazil during the period. This headline estimate is quantitatively plausible: it implies roughly a 1% increase in mortality risk per 10 $\mu g/m^3$ of particulate pollution, on the same order as prior estimates. For example, Deryugina et al. (2019) report an elasticity of around 1.8% for the U.S. elderly population. Our estimate is likely conservative: we focus on contemporaneous mortality responses, whereas the long-term effects of pollution exposure are typically larger (Ebenstein et al., 2017), and we do not account for non-fatal health damages such as morbidity or reduced labor productivity (Graff Zivin and Neidell, 2012; Borgschulte, Molitor, and Zou, 2022).

We make three contributions to the literature. First, we quantify the causal impact of trade on deforestation. Tropical deforestation remains a critical environmental challenge, with implications for climate change and biodiversity loss (Balboni et al., 2023). While the trade and environment literature has traditionally focused on the role of industrial emissions, there is a growing body of work that examines the environmental impact of trade through its interaction with natural resources. In particular, recent research explores how trade liberalization affects land use and forest cover (Harstad 2024; Farrokhi et al., 2024). To the best of our knowledge, this paper provides among the first causal estimates on the impact of exports on deforestation. The most closely related work is Carreira, Costa, and Pessoa (2024), who study the impact of agricultural productivity changes and China shocks – and their interactions – on forest cover in Brazil.[3] Earlier work such as Ferreira (2004) also documents a negative relationship between

[3] Carreira, Costa, and Pessoa (2024) identify a strong negative impact of new agrotechnology (genetically engineered soy seeds) on forest cover in Brazil, along with a negative, though less statistically robust, effect from trade shocks. Our findings on trade-driven deforestation in Section 4 align broadly with their results, though our approach differs in two key ways. First, instead of focusing solely on demand shocks from China, our instrumental variable captures agricultural demand variation from multiple major importing countries. Second, we use a more extensive dataset with additional years and refined satellite measurements of forest cover, likely enhancing the precision of our estimates.

trade and forest cover, though mostly based on cross-country comparison without causal identification.[4]

Second, we add to the literature on the environmental and health effects of forests. This literature is nascent in itself, but emerging applications have found important implications of forest presence on weather, climate, agriculture, infectious diseases, health, among other social economic outcomes such as property values (Berazneva and Byker, 2017, 2022; Garg, 2019; Jones and Goodkind, 2019; Druckenmiller, 2020; Han et al., 2021; Arujo, 2023; Grosset-Touba, Papp, and Taylor, 2023; Li, 2023; Xing et al., 2023). Our study is the first to identify a direct link between forests and mortality rates, adding a significant dimension to the costs associated with forest loss, and doing so across a wide, inter-city geographical scale. By quantifying how forests safeguard human life via pollution reduction, we highlight an immediate public health value of forest conservation that complements the longer-run climate and ecosystem values.

Third, we formally link trade, deforestation, and health, identifying natural capital depletion as an important yet overlooked channel through which trade affects welfare. Prior research has recognized that trade shocks can influence health through income channels or through changes in local pollution emissions. For example, trade-induced job loss has been shown to increase drug overdoses (Pierce and Schott, 2020), reduce access to employment insurance (Guerrico, 2021), and worsen workers' physical and mental health (Adda and Fawaz, 2020). Bombardini and Li (2020) show that Chinese cities specializing in dirty industries experience both pollution and income effects, leading to increases in mortality. In contrast, cities specializing in clean industries only enjoy income effects and experience decreases in mortality. Gong et al. (2023) examine how foreign demand shocks due to the global economic crisis reduce demand for Chinese products, drive local changes in air quality, and affect mortalities. Tanaka, Teshima, and Verhoogen (2022) analyzes the effect of a U.S. air-quality standard on cross-border battery-recycling flows and finds that recycling shifted from the United States to Mexico which in turn led to increased lead exposure and worsened infant health outcomes near Mexican plants We extend this literature by emphasizing the role of natural capital—in our case, the Amazon forest—as an important determinant of population health. Our analysis shows that trade-

[4] See also Andela et al. (2017) and Curtis et al. (2018) for cross-country estimates. The general link between agricultural expansion and deforestation is more extensively studied. See, for example, Busch and Ferretti-Gallon (2017), Assunção et al. (2020), Heilmayr et al. (2020), and Penderill et al. (2022).

induced depletion of this natural resource can substantially undermine the net social benefits of trade, by imposing large health externalities on distant communities that are typically omitted from conventional trade benefit–cost calculations.

More broadly, our work provides a quantitative basis to account for the environmental externalities of trade and the value of ecosystems like forests in economic policy analysis. Policymakers have only a limited set of tools (e.g. domestic environmental regulations or conservation policies) to mitigate the natural capital depletion associated with trade-driven growth (Copeland, Shapiro, and Taylor, 2022). Designing effective policy responses requires rigorous evidence that monetizes the value of natural assets, and our study offers one feasible framework to do so.[5] In addition to providing an overall estimate of the export-health trade-off, our estimates may also be useful for targeting, e.g., identifying areas where the same amount of deforestation would lead to the largest downwind environmental health damage. This opens new possibility for more informed discussions on balancing the economic gains from trade against the often hidden health costs of environmental degradation.

Section 2 continues with institutional knowledge on trade, deforestation, the environment, and human health. Section 3 describes the overall research framework and data sources. Section 4 presents the causal estimation of the effect of export on forest coverage. Section 5 presents the health analysis. Section 6 presents the cost calculation and concludes the paper.

2. Institutional Background

2.1 Agricultural Export and Deforestation in Brazil

Brazil is the eighth largest economy and the world's seventh most populous country. At the same time, Brazil is an ecological hotspot, home to 60 percent of the Amazon rainforest and the Cerrado biome, the world's most biodiverse tropical savannah. It is estimated that Brazil holds about 10 percent of the world's known biodiversity (Lewinsohn and Prado, 2005). In the

[5] See, for example, Recommendation 3 of *National Strategy to Develop Statistics for Environmental-Economic Decisions*, Office of Science and Technology Policy, Office of Management and Budget, Department of Commerce (2023). In addition to direct regulations, many alternative methods for fighting deforestation may also benefit from concrete estimates of health effects of forest losses, such as conservation contracting and ecosystem payment programs (Jayachandran et al., 2017; Harstad, 2024).

shadow of the rapid expansion of agribusiness in Brazil, deforestation is emerging as an environmental crisis. In many developing countries, including Brazil, farmers are driven to deforest land as a means to increase their agricultural output and income. The prevalent method of land conversion involves slash-and-burn techniques, where trees are cut down and the remaining vegetation is burned, enriching the soil with nutrients from the ash. The opening of new lands for agriculture is frequently facilitated by government subsidies or lax enforcement of environmental regulations, further incentivizing farmers to engage in these practices (Fearnside, 2005).

The interplay between agricultural expansion and deforestation is particularly evident in the Brazilian Amazon Rainforest and the Cerrado, where the cultivation of soybeans and the expansion of cattle ranching are the primary agricultural activities driving deforestation (Song et al., 2021). Soybeans, a major export crop, have seen increased demand globally, particularly from China and the European Union, for use as livestock feed and in various food products. This demand has propelled Brazilian farmers to clear vast tracts of the Amazon to cultivate this lucrative crop. Similarly, cattle ranching, which requires extensive land area for grazing, has expanded dramatically, making Brazil one of the world's largest beef exporters. The profitability of these agricultural ventures, along with insufficient regulatory enforcement and government policies that frequently favor economic growth over environmental protection, is widely regarded as a major driver of significant deforestation in the region (Barona et al., 2010).

Weak enforcement of environmental laws has further exacerbated deforestation. Brazil's Forest Code mandates that private landowners conserve a portion of their land under native vegetation—80% in the Amazon biome with the remaining 20% allowed for clearing (Brazil WWF, 2016). Compliance with these rules is ostensibly monitored through various programs, including the use of advanced technologies such as satellite remote sensing (Mullan et al., 2022). In practice, however, those caught illegally clearing forests often face limited consequences. The Brazilian Institute of Environment and Renewable Natural Resources (IBAMA), the federal environmental enforcement agency, can issue fines and embargoes on illegally deforested land, and severe cases may be prosecuted with potential jail time for offenders. Yet bureaucratic delays and legal appeals have frequently blunted the effectiveness of these enforcement tools: by 2020, fewer than 10% of environmental violation cases had resulted in a fine being paid. This lack of effective punishment likely has eroded the deterrent power of the regulations (Nunes et al., 2024).

2.2 Forests and the Environment

Forests represent a crucial component of natural capital, contributing to the ecosystem and the environment. They function as indispensable habitats for 80% of the global terrestrial species (Aerts and Honnay, 2011). Besides, forests contribute to water, oxygen, and carbon cycles, and other biogeochemical balances. They also play a pivotal role in the global and local climates. Forests are the world's largest storehouses of carbon. Trees absorb greenhouse gasses, and are primary instruments for carbon storage featured in carbon offset programs like the REDD+. At the local level, forests affect micro-climate via shading and evaporation (Bonan, 2008; Pan et al., 2011).

Forests matter a lot for human well-being. Over 1.6 billion people depend on forests for food, fuel, or shelter, and 70 million people including indigenous communities rely on forests for settlement (UN, 2021). Forests also mitigate damages from pollution and natural disasters such as floods. In this paper, we focus on air pollution impacts of forests as short-term consequences of trade-induced deforestation. Unlike other effects, air pollution responds quickly to tree cover change and could be linked to export changes of interest. Air pollution also leads to immediate mortality responses, enabling us to quantify health externality.

Forests mitigate air pollution through several mechanisms. First, leaves and bark act as natural filters for particulate matter, providing deposition surfaces for airborne pollutants. Studies show that forests efficiently capture particulate pollution, thereby improving air quality (e.g., Betts et al., 2008; Janhall, 2015). Second, foliage absorbs harmful gases such as SO_2, NO_x, and O_3 and chemically interacts with them. Leaves can also biodegrade or transform certain pollutants into less toxic forms (Wei et al., 2017). Third, trees alter the local microclimate in ways that suppress the formation and persistence of pollution. For example, cooler temperatures in forested areas inhibit ground-level ozone formation (Coates et al., 2016), and higher humidity and rainfall promote the removal of particulate pollutants from the atmosphere.

Importantly, the deforestation–air pollution–health link is not confined to local areas, because wind can transport pollutants over long distances. Prevailing winds carry pollution from upwind deforestation zones to downwind regions, so wind speed and direction determine how far pollution travels and how long it lingers. Prior research has documented significant

transboundary air pollution impacts on downwind areas (e.g., Heo, Ito, and Kotamarthi, 2023). As a result, deforestation in one location—such as clearing land for export agriculture—can degrade air quality and public health in communities far downwind. Recognizing the protective role of forests, policymakers have implemented afforestation projects to help shield downwind populations from air pollution. For example, China's Three-North Shelter Forest is a vast windbreak intended to reduce dust storms from the Gobi Desert and improve air quality near the capital region (Bryan et al., 2018).

3. Research Framework and Data

3.1 Research Framework

Before proceeding, it is worth laying out how various parts of our empirical estimation are eventually going to line up. Our goal is to estimate the external health effects of trade-induced deforestation that occurs in city i, recognizing that this effect need not confine locally to where deforestation occurs. The empirical analyses can be thought of as being organized around the following conceptual equation:

$$\text{Health Effects}_i = \sum_r \underbrace{\frac{\partial \text{Forest}_i}{\partial \text{Trade}_i}}_{\text{Section 4}} \cdot \underbrace{\left(\frac{\partial \text{Health}_r}{\partial \text{Forest}_i} \middle| \overbrace{\text{Wind}_{i \to r}}^{\text{Section 5.1}} \right)}_{\text{Section 5.2}} \quad (1)$$

Section 4 estimates the causal effect of trade on deforestation ($\frac{\partial \text{Forest}_i}{\partial \text{Trade}_i}$). This estimate is entirely local in nature: we want to learn how much of city i's deforestation is due to trade shocks to *that* city. Section 5 estimates the spillover health effects of city i's deforestation on all potential "receiver" cities indexed by r. Section 5.1 first builds an algorithm that identifies these potential receivers. We use high-frequency wind direction information to create a downwind exposure index $\text{Wind}_{i \to r}$ which summarizes the degree to which city i may have an influence on city r's environmental condition due to atmospheric motions. Section 5.2 then builds on this information to estimate the relationship between city i's forest cover and receiver city r's health outcomes – which we show is highly dependent on, and nonlinear with respect to, the downwind exposure index. The total effect of city i's is thus the summation across its effects on various downwind

receiver cities. In Section 6, we come back to an empirical version of equation (1) to derive our headline, cost-of-trade-induced-deforestation number.

Equation (1) also makes clear that our analysis focuses specifically on one mechanism linking trade to health, rather than attempting to capture the full spectrum of trade's economic, environmental, and health effects. Our goal is to quantify the health externality transmitted via trade-induced deforestation and long-distance pollution transport. Trade can also influence health through other channels – for example, by raising incomes, improving healthcare access, or spurring infrastructure development – which lie beyond our scope. By isolating this deforestation–pollution–health pathway, we highlight an important but previously overlooked channel without making broad claims about trade's overall welfare effects.

3.2 Data

Exports. Our export data is from the Comex database provided by Brazil's Foreign Trade Secretariat (Secretaria de Comércio Exterior - Comex). The original data is at the municipality by month level and is structured using the Harmonized System at the 4-digit level ("HS-4"), providing detailed categorization of exported goods. We have access to data between 1997 and 2019.

Brazil's export data report the municipality of origin as the fiscal domicile of the exporting firm, not necessarily the production site. This can misalign recorded export locations with where commodities are actually produced. This reporting convention is consistent across sectors, though its impact varies: it is most distortive for industries with exporters headquartered far from production, and less so for agriculture where many exporters (e.g. cooperatives) are based near farming areas. Agribusiness supply chains are also regionally anchored, so the municipality-of-record for, say, soy or beef exports is usually within the producing zone. To alleviate this concern, we aggregate the municipal export data to Minimum Comparable Areas (AMC) regions which merge municipalities into stable units. Aggregation helps realign exports with production areas by capturing cases where an exporter's city and the production hinterland are in the same broader region.

Land Use. Our land use data is from MapBiomas. Based on the Landsat satellite images produced by NASA and USGS, MapBiomas processes the pixel-per-pixel data with machine

learning algorithms through the Google Earth Engine platform. It produces annual land use and land cover maps and provides information on the dynamics of different types of land cover for Brazil from 1985 to 2022 on a 30m spatial resolution. Specifically, there are six types of land, namely forest, non-forest natural formation, farming, non-vegetated area, water, and not observed. We mainly analyze the data on forest land and farming land. There are four types of forest lands, namely forest formation, savanna formation, mangrove, and sandy coastal plain vegetation. There are four types of farming land, namely pasture, agriculture, forest plantation, and mosaic of uses. For agricultural land, the MapBiomas offers information on major crops, such as soybean, sugar cane, rice, cotton, coffee, and citrus. The data used in our paper is the 7.0 version obtained in 2022.

Meteorology. We draw daily temperature and precipitation data from BDMEP (Banco de Dados meteorológicos para Ensino e Pesquisa). Between 2000-2015, BDMEP provided data from 150 weather monitoring stations. The network expanded to include 5,611 stations for the years 2016-2020. For each station-day, we observe daily minimum and maximum temperatures (°C) – from which we calculate average temperature by taking the average of the two – and precipitation (mm). We then compute station by month average temperature and precipitation. To derive city-level weather variables, we match all weather stations within a 300-kilometer radius of each city's centroid and calculate the average temperature and precipitation across these matched stations.

We use wind direction and speed data from the European Centre for Medium-Range Weather Forecasts Reanalysis 5 (ERA5) reanalysis product. This dataset provides hourly U (eastward) and V (northward) components of the wind vectors at a 0.25° grid resolution. We use this data to compute daily prevailing wind directions, which are used in the air flow analysis in Section 5.

Air Quality. Air quality data is sourced from IEMA (the Instituto de Energia e Meio Ambiente). It contains hourly air quality monitoring data from 380 stations in 28 cities from 2015-2022. The IEMA data keeps track of six different air pollutants: fine particulate matter ($PM_{2.5}$), coarse particulate matter (PM_{10}), ozone (O_3), nitrogen dioxide (NO_2), sulfur dioxide (SO_2) and carbon monoxide (CO). Because trees can mitigate both particulate and gaseous pollutants (Section 2.2), rather than focusing on these pollutants individually, we compute the z-scores for each of the six pollutants and then average these z-scores to construct an overall air pollution index. This index serves as our primary measure of air quality in the regression analysis.

Regression results using individual pollutant concentrations as the outcome variables are available in the Online Appendix Figure 8.

Forest Fires. We use fire data from NASA's Fire Information for Resource Management System (FIRMS), which derives fire detection from the MODIS Fire and Thermal Anomalies product covering the period 2000–2022. The MODIS instrument identifies active fire hot spots at a spatial resolution of 1 km and a daily temporal frequency, detecting both natural and anthropogenic fires, whether intentional or accidental. Each detection includes the geographic coordinates (at 1 km resolution) and the date of occurrence. We aggregate the number of active fire detections to the microregion-by-month level for analysis.

Mortality. We obtain mortality microdata from the Mortality Information System (Sistema de Informações sobre Mortalidade, or SIM) via the Brazilian National Health System Information Technology Department (Departamento de Informática do Sistema Único de Saúde, DATASUS). The SIM data are derived from administrative death records, which are completed and issued by physicians, and collected from hospitals and medical examiner offices.

From the death record microdata, we observe the decedent's municipality of residence, date of death, and the underlying cause of death coded in ICD-10 classification. Using these information, we aggregate the microdata to obtain death counts at the microregion-by-month level between 2000-2021.[6] We categorize deaths into those due to cardiovascular or respiratory causes ("cardiovascular", ICD10: I00-I99, J00-J99) and all other, non-cardiovascular causes. Separately, we count deaths due to accidents ("external", ICD10: S00-T98, V01/V989), which we will use as a "placebo" outcome in our econometric analysis. Finally, we convert death counts to death rate by dividing microregion level population counts from the Brazilian Institute of Geography and Statistics.

Geography. Because municipality boundaries changed over time over our study period, and to address potential misalignment between exporting and production location in the COMEX data (as mentioned earlier in this section), we aggregate geographic units to the 3,826 Minimum Comparable Areas (henceforth "AMC" area) level for temporal consistency (Ehrl, 2017). We drop

[6] The SIM mortality data began in 1997, although we drop data from 1997 to 1999 due to missing information on causes of death.

five municipalities that cannot be identified in the municipality-to-AMC crosswalk.[7] Our primary trade-deforestation analysis is based on AMC-level data. Our environmental data have a coarser resolution than AMCs (e.g., 0.25 degree for wind, 380 air quality stations). Therefore, in airflow modeling and the subsequent environmental health analysis, we aggregate AMCs into 557 "microregions" – which we will henceforth refer to as "cities" – as defined by the Brazilian Institute of Geography and Statistics.

4. Trade, Agricultural Expansion, and Deforestation

4.1 Raw Statistics

We begin with summary statistics on Brazil's agricultural export growth, land-use change, and deforestation over the study period. Figure 1, panel (a) shows that Brazil's annual agricultural export value quadrupled from around 20 billion USD in 1997 to over 80 billion USD by 2018. Appendix Figure 1 panel (a) shows distribution of export values across agricultural products. Appendix Figure 1 panel (b) shows that the increase in exports is mainly driven by rising demand from China and the EU. Appendix Figure 3 shows that this export boom was concentrated in traditional farming regions: the geographic distribution of agricultural export growth indicates that the largest increases occurred in areas with substantial crop production, a pattern mirrored by notable agricultural employment gains in those same regions. By contrast, Appendix Figure 4 shows that growth in mining exports – the other main sector that saw substantial growth during the study period – followed a very different spatial pattern, suggesting that the regions experiencing deforestation were responding primarily to agricultural export shocks.

Figure 1, panel (b) shows the corresponding land-use changes. Brazil's forest cover declined steadily over the past two decades, almost one-for-one with an expansion in farmland area. The map on the right side of the panel highlights that deforestation was most pronounced in the same regions that saw large agricultural export gains. Consistent with this, Appendix Figure 2 shows that the municipalities with the greatest farmland expansion (for example, in Mato Grosso and the Amazon frontier) also suffered the largest forest losses. Table 1 presents

[7] Mojuí dos Campos, Pescaria Brava, Balneário Rincão, Pinito Bandeira, and Paraíso das Águas.

more summary statistics of key variables used in our analysis. We next turn to an empirical strategy to identify the causal effect of export growth on land use.

4.2 Research Design

The main estimation equation to estimate the causal impact of trade shocks on deforestation and land use is as follows:

$$\Delta\text{Land Cover}_{i,y} = \beta \cdot \Delta\text{Export}_{i,y} + \lambda \cdot W_{i,y} + \varepsilon_{i,y} \quad (2)$$

where $\Delta\text{Land Cover}_{i,y}$ is the four-year rate of change in a certain type of land cover at AMC area i and year y. For example, when the outcome of interest is deforestation, the land cover variable is defined as $\Delta\text{Forest}_{i,y} = (\text{Forest}_{i,y+4} - \text{Forest}_{i,y})/\text{Land}_{i,y}$ where "Forest" denotes forest cover in acreage in the area-year, and "Land" is total area land size. We use a four-year differencing period in both equation (2) and in the construction of our instrumental variable below. We will present robustness checks with alternative differencing windows, ranging from one to six years. We chose the four-year period as our primary specification because the magnitude of the estimated effect stabilizes from this point onward, suggesting that a four-year window is sufficiently long to capture the temporal dynamics between export shocks and deforestation activities.

The key right hand side variable $\Delta\text{Export}_{i,y}$ is the four-year change in agricultural exports per capita. $W_{i,y}$ is a series of control variables, including macro-region fixed effects, year fixed effects, and region-time control variables including income per capita, literacy rate, rural population, urban population, population density, and the presence of genetically-modified soy.[8] The coefficient of interest β therefore captures the impact of agricultural export growth on land cover changes. We cluster standard errors at the AMC level. All regressions are weighted with each AMC's agricultural population in year y.

Simple OLS estimation of equation (2) may suffer from endogeneity and measurement errors. We build the following shift-share instrumental variable (IV) for the export variable:

[8] We follow Carreira, Costa, and Pessoa (2024) in selecting these control variables. Our estimates are insensitive to the exclusion of these covariates.

$$IV_{i,y} = \left[\sum_j \frac{Export_{i,j,t-4}}{Export_{i,t-4}} \cdot \frac{Import_{j,t+4} - Import_{j,t}}{(Import_{j,t+4} + Import_{j,t})/2}\right] \cdot \frac{Export_{i,t-4}}{Pop_{i,t-4}} \quad (3)$$

where $Export_{i,j,t-4}/Export_{i,t-4}$ is the "share" of product j in AMC area i's exports at period $t-4$, which captures an area's historical export of a certain type of agricultural product. $Import_{j,t}$ is major importing countries' total import from the world in product j and year t, which measures the global import demand for product j. The term $\frac{Import_{j,t+4} - Import_{j,t}}{(Import_{j,t+4} + Import_{j,t})/2}$ therefore captures percent change (or "shift") in product demand over the period of interest. Together, the shift-share terms in brackets of equation (3) capture the variation in an area's exposure to global demand shocks due to historical differences in export capacity across product categories. To express the IV variable in terms of per-capita dollar value – consistent with the endogenous variable in equation (2) – we multiply by $\frac{Export_{i,t-4}}{Pop_{i,t-4}}$, which represents area i's overall historical export exposure. Because the export values of many products are zero in early years, it is not possible to calculate growth for some products. To address this issue, we construct the modified version of import growth following Davis and Haltiwanger (1992), where the denominator is the average of the start-of-period value and end-of-period value. Appendix Table 1 lists the major importing countries and products used in constructing the instrument.

The shift-share IV strategy relies on trade shocks being (i) diverse, uncorrelated across product categories, and (ii) as-good-as-random conditional on shock-level unobservables and exposure weights (Borusyak, Hull, and Jaravel, 2022). Several empirical facts and tests support these assumptions.

First, Brazil's agricultural export base is highly diversified: between 1997 and 2019, Brazil exported over 190 distinct agricultural products (at the HS-4 level), with an average Herfindahl–Hirschman Index of 0.07, indicating very low concentration. Second, import demand growth varies widely across products – Appendix Figure 5 shows that different crop categories experienced markedly different demand trajectories. These facts imply that our instrument draws on a large number of disparate shocks rather than any single dominant trend, making it unlikely that one particular commodity shock drives the results.

The exogeneity of trade shocks cannot be tested directly. Following Borusyak, Hull, and Jaravel (2022), we conduct a balancing test on whether the instrument is correlated with pre-existing regional trends or characteristics. Specifically, we regress pre-shock observable

characteristics on the IV variable, controlling for the same set of fixed effects variables as in equation (2). We look at control variables that we used as covariates in equation (2), as well as climate variables such as temperature, precipitation, and humidity which might correlate with agricultural suitability. Table 2 shows that the IV variable does not significantly correlate with these predetermined characteristics.

In additional robustness checks, we address potential endogeneity in the construction of the trade shocks themselves. One potential concern is that supply shock in Brazil (say, a drought reducing soy output) could impact international prices and quantities and thus appear as an import demand "shock" for that product. To alleviate this, we modify the instrument construction in two ways. First, we exclude Brazil's own exports when calculating the world import growth for each product, so that the shock is driven purely by foreign demand. Second, we purge any common component of shocks at the broader product-group level: before computing the instrument, we residualize each product's import growth with respect to HS-2 category fixed effects, using only the remaining idiosyncratic variation in demand. These modifications likely understate the true demand shock magnitudes, but they help reduce any scope for reverse causality. Reassuringly, our results are robust to using this alternative IV construction (see Appendix Table 2).

Another potential concern with shift–share designs is that if regions have similar export structures, they may experience correlated shocks, which can lead to over-rejection of the null in inference. We follow Adão, Kolesár, and Morales (2019) and conduct a placebo test, where we simulate shift-share IV variables with shift shocks randomly drawn from a normal distribution with mean 0 and variance 5. We then estimate the reduced form effect by regressing forest growth on the placebo IV, repeating this procedure 1,000 times. To assess overrejection, we examine rejection characteristics in the distribution of placebo coefficients. Appendix Figure 6 shows that the placebo regressions render significant results approximately 10.6% of the time at the 5% significance level and 1.5% of the time at the 1% significance level. This suggests that our inference is not unduly biased by correlated shocks across regions, and that the conventional clustered standard errors are appropriate in our setting.

4.3 Results

Figure 2 reports the primary estimates. Each node on the tree represents a separate regression. All regressions follow the exact same IV specification as laid out in equations (2)–(3), except for the outcome variables which are denoted by the name of the node. Branches of the tree represent hierarchies of the land use variables defined in the MapBiomas dataset. For example, the "forest" land use category consists of four subcategories: "forest formation," "savanna formation," "mangrove," and "sandy." The values on the four sub-nodes represent the causal impacts of export on each subcategory, which collectively sum to the overall causal impact on the main forest node. We find that the total deforestation effect is driven mainly by reductions in the "forest formation" and "savanna formation" subcategories (i.e., primary forests and woody savannas), with minimal changes in mangrove or sandy cover.

The headline "export-deforestation" estimate of this paper is shown on the "ΔForest" node of the figure: each 1,000 BRL increase in export per capita reduces forest cover by 0.174 percentage points. This estimate is statistically significant at the 5 percent level, and the effect size converts to about 5.7 percent of a standard deviation (S.D.) reduction in forest cover per 1 S.D. change in export. Consistent with the sub-node breakdown mentioned above, this total deforestation effect is driven mainly by decreases in forest and savanna formation.

Turning to the lower parts of the graph, we find that export leads to significant increases in total farmland coverage by about 0.214 percentage points. This effect is diluted by the fact that, in the land use data, "forest plantation" is counted toward farming activities, which – consistent with our deforestation results above – is negatively affected by exports. The smaller net gain in overall farmland relative to the larger increase in cropland (0.334 percentage points) suggests some land use substitution – for example, part of the new crop expansion comes from converting existing pasture or mixed-use land to row crops, rather than exclusively clearing new forest land. This indicates that export booms can induce both extensification (clearing forests for new farms) and intensification (repurposing previously cleared land toward higher-value crops), consistent with well-known patterns in Brazilian agriculture.

We can further look at which crop types drive the agriculture effects. The right-hand side parts of the graph show that export's effect on agriculture is driven primarily by an increase in soybean farming. Indeed, soybean cultivation accounts for the bulk of the export-induced

expansion in crop area, which is consistent with Brazil's dominant role in global soy markets. The prominence of soy-driven deforestation has been a focal point of policy discussions in Brazil – for example, the 2006 Soy Moratorium in the Amazon biome was introduced to curb forest clearing for soybean fields. Our results empirically confirm that soybean export demand was a key driver of land use change, which reinforces the importance of such policy measures.

Finally, it is worth noting that our choice of a four-year differencing window was guided by stability of the coefficient. Table 3 shows that using shorter windows yields smaller immediate effects, whereas beyond four years the cumulative effect plateaus. This suggests that deforestation in response to an export shock can play out over several years, but most of the impact materializes within a four-year period. The consistency of the estimates across these checks provides confidence in the stability of the export–deforestation relationship.

5. Health Effects

5.1 Area-of-Effect Modeling

To capture downwind environmental and health effects, we build a matrix that summarizes monthly wind flow intensities between all pairs of cities in Brazil. In the interest of space, here we provide an intuitive explanation of the procedure, leaving computational details to the Online Appendix.

Model. The input data are 0.25-degree resolution by hourly wind direction and speed information (i.e., vectors) from the ERA5 product. We first generate a spatial representation of wind *flows* from individual wind *vectors*, as illustrated in Figure 3a. Beginning from a particular day and city, we construct streamlines by sequentially following the wind's speed and direction on a daily basis. This process maps out the evolving trajectories of the wind field, giving us daily representations of the distribution of wind flows throughout the country.

Our goal is to build an index, $\text{Wind}_{i \to r,d}$, which is a summary of downwind intensity blowing from a sender city i to a receiver city r on day d. Note that, for any pair of cities that are significantly distant from each other, it is meaningless to talk about up/downwind relationship on any given "day" because winds blowing from the sender city may take days to arrive at the receiver city. We therefore track the trajectory of winds "originating" from a sender city and their

impacts of downwind cities over multiple days – or "steps" as we refer to them below – using the wind streamline data that we constructed earlier.

We define downwind intensity score using the following formula:

$$\text{Wind}_{i\to r,d,t} = \exp\{-\alpha \cdot \text{rad}_t - \beta \cdot |\theta|_{i\to r,d,t} - \gamma \cdot \text{dist}_{i\to r,d,t}\} \quad (4)$$

Starting from sender city i on day d and at step t, we assume downwind intensity of receiver city r follows an exponential decay as a function of three components (U.S. EPA, 2018; Phillips et al., 2021). The first component is the search radius at the step (rad_t), which captures general decreases of downwind intensity over steps. The initial radius is 300 km, and we increase the search radius by 20 km at each step to capture both the uncertainty in the streamline computation and the dispersion of air. The second component is the scalar product of the angle between the receiver city and the wind direction originating from the sender's location ($|\theta|_{i\to r,d,t}$), which means we assign higher intensity to receiver cities that sit closer to the exactly-downwind direction of the sender. The third component is simply the distance between the sender and the receiver city ($\text{dist}_{i\to r,d,t}$), which captures geographic decay. We assume $\text{Wind}_{i\to r,d,t}$ to be zero if $d_{i\to r,d,t} > \text{rad}_t$ (i.e., if receiver city lies outside of the search radius at step t) or if $\theta_{i\to r,d,t} > 0.4\pi$ (i.e., if the receiver city is not obviously in the downwind direction from the sender city.[9] Starting from each particular sender city and day, we iterate the procedure for seven steps (i.e., a week).

Perhaps an easier way to think about the procedure above is that, we essentially "move" the location of the sender city with the wind flow and see which receiver cities it touches along the path over the next week period. A visualization of the procedure is shown in Figure 3b. The red arrow at the center represents the locus of the wind flow starting from the sender city. The growing ball of uncertainty around the arrow shows expanding search radius rad over steps in equation (4). The visualization also explains why both the relative angle and distance variables (θ and dist) have starting day and step subscripts (d and t): we track where winds originate and where they move to, and we compute each receiver city's relative angle and distances dynamically.

[9] We use parameter values $\{\alpha, \beta, \gamma\} = \{0.7, 0.5, 0.2\}$. These numbers are empirically determined such that we would obtain a spatially continuous flow coefficient function through the successive steps, and that the directionality of the observed winds are respected through the flow coefficient representation. See Online Appendix for more details.

We aggregate step-wise downwind intensity scores to the day level:

$$\text{Wind}_{i\to r,d} = \sum_t \text{Wind}_{i\to r,d,t} \quad (5)$$

and in the econometric analysis below, we further average this city pair-daily score to the monthly frequency ($\text{Wind}_{i\to r,m,y}$ where the variable is indexed by month m, and year y) to make the size of the regression dataset manageable. Because the numerical values of these scores lack direct contextual meaning, in econometric analysis we use a nonparametric approach, grouping this variable into decile bins for positive values plus a separate bin for when downwind score is zero (i.e., because the receiver city is too far away or it is not in the downwind direction, as discussed earlier).

Validation. Estimating atmospheric transport between cities is a complex task, but the model we outlined above is deliberately parsimonious. This naturally raises the question of whether it is sufficient to capture long-range air movement. We propose a validation test: we examine whether our downwind index predicts pollution passthrough from upwind to downwind cities. Specifically, we focus on fine particulate matter (PM2.5), which is well known to travel long distances, and test whether a receiver city's pollution more closely resembles that of its upwind counterpart when the corresponding downwind intensity score is high. Importantly, because pollution data were not used in constructing the downwind intensity scores, this test provides an independent validation of the model's ability to capture atmospheric transport.

We model the passthrough between $\text{Pollution}_{i,m,y}$ and $\text{Pollution}_{r,m,y}$ – particulate matter pollution levels at the sender city i and at the receiver city r in month m and year y – as a function of the associated downwind intensity score between the city pair, $\text{Wind}_{i\to r,m,y}$. We estimate the following regression equation:

$$\text{Pollution}_{r,m,y} = \beta \cdot \text{Pollution}_{i,m,y} \times \text{Wind}_{i\to r,m,y} + \gamma \cdot \text{Wind}_{i\to r,m,y} + \alpha_{i,r,m} + \alpha_y + \varepsilon_{i,r,m,y} \quad (6)$$

where $\text{Wind}_{i\to r,m,y}$ is specified as a categorical variable comprising 11 groups: ten decile bins for non-zero downwind scores and an additional bin for zero wind values, representing "calm" conditions where no downwind relationship is observed between the two cities. We omit the main effect of $\text{Pollution}_{i,m,y}$ from the regression, so that the origin-to-destination pollution passthrough β coefficients can be identified for each of the 11 downwind score bins. Equation (6) includes sender-by-receiver-by-month-of-year fixed effects ($\alpha_{i,r,m}$). The identifying variation thus

comes from within sender-receiver-seasonal pairs across different years, where variations in wind intensities are plausibly exogenous. We also include year fixed effects (α_y) to account for common shocks at the year level. Standard errors are two-way clustered at both the sender and receiver levels.

Figure 4 reports the β estimates. We find strong sender-to-receiver PM2.5 passthrough when the modeled downwind intensity is high, with a monotonic decline in passthrough as the downwind score decreases. Reassuringly, the passthrough effect is near zero when the modeled downwind intensity is zero (i.e., under "calm" conditions). In other words, we observe substantial pollution transmission when our model predicts strong atmospheric connectivity, and little to no transmission when it predicts none. Taken together, these results provide validation that our downwind index effectively captures the potential extent of pollution transport between cities.

5.2 Research Design

Our goal is to estimate the relationship between a sender city's quantity of forests and its downwind receiver's environmental and health outcomes, leveraging month-to-month fluctuations in the downwind score (as illustrated in Figure 3b). Our estimation equation is as follows:

$$Y_{r,m,y} = \beta \cdot Forest_{i,y} \times Wind_{i \to r,m,y} + \gamma \cdot Wind_{i \to r,m,y} + \alpha_{i,r,m} + \alpha_y + \varepsilon_{i,r,m,y} \quad (7)$$

Equation (7) mirrors the structure of Equation (6), with the only difference being that the upwind pollution variable is replaced by the amount of forest cover in the upwind area. A unique observation in our estimation data is indexed by sender city (i), receiver city (r), month (m), and year (y). The three key variables in this estimation equation are: $Y_{r,m,y}$, which is the receiver city's outcome in a given month; $Forest_{i,y}$, which is the sender city's forest acreage in the corresponding year (standardized to mean zero and standard deviation one) multiplied by minus one to capture the effects of losses; and $Wind_{i \to r,m,y}$, which is the downwind score reflecting strength of wind blowing from i to r in that month. Like in equation (6), we categorize the $Wind_{i \to r,m,y}$ variable into 11 groups: 10 decile bins for non-zero downwind scores and one additional bin for zero wind scores representing "calm" conditions with no downwind relationship between the two cities.

We then include $\text{Wind}_{i\to r,m,y}$ as a categorical variable in the regression, and so there is one β coefficient for each of the 11 downwind score bins. We include sender by receiver by month-of-year fixed effects ($\alpha_{i,r,m}$), which isolate downwind variation arising within a city pair *and* month of the year to address potential cross-sectional and seasonal confounds. For example, consider the city pair of Sao Paulo and Brasilia. Our specification compares a particular January when the wind blowing from Sao Paulo to Brasilia is particularly strong with other Januaries in different years when the wind strength for the same city pair is comparatively weaker. This strategy enables us to parse out cross-sectional correlations (e.g., the fact that downwind relationships tend to be generally stronger for city pairs where the two cities are in close proximity) and city pair-specific seasonality of wind patterns. We also include year fixed effects (α_y) to account for common shocks at the year level. In all regressions, we two-way cluster standard errors at the sender and receiver levels.

Our coefficients of interest are the β's, which capture the relationship between upwind forest losses and downwind environmental or health condition at varying levels of wind intensity blowing from the upwind to the downwind city. We hypothesize that at high levels of wind intensity, the coefficient should be positive, indicating that forest losses in the upwind city increases pollution and mortality in the downwind city. As wind intensity decreases, we expect this relationship to weaken. The coefficient estimated under "calm" conditions (i.e., no wind between the city pair) serves as a placebo test: without wind, we anticipate no relationship between upwind forest cover and downwind pollution or health outcomes.

A potential alternative explanation for the observed relationship between upwind forest cover and downwind pollution and mortality is a fire channel, where land-clearing fires—a common method for deforestation and farmland conversion—generate air pollution that drifts downwind, thereby degrading air quality and creating a spurious negative relationship between upwind forest cover and downwind pollution. To examine the relevance of this mechanism, we incorporate remote-sensing data on fire activity in upwind cities and modify equation (7) by including a full interaction of upwind fire activity with downwind wind exposure bins. The augmented specification is:

$$\begin{aligned} Y_{r,m,y} = \beta \cdot \text{Forest}_{i,y} \times \text{Wind}_{i\to r,m,y} + \theta \cdot \text{Fire}_{i,m,y} \times \text{Wind}_{i\to r,m,y} \\ + \gamma \cdot \text{Wind}_{i\to r,m,y} + \alpha_{i,r,m} + \alpha_y + \varepsilon_{i,r,m,y} \end{aligned} \quad (8)$$

Here, $Fire_{i,m,y}$ captures the number of fire spots in the sender city during the month, measured based on satellite observations (Section 3.2). Equation (8) effectively tests a "horserace" between the effects of forest cover and fire activity in upwind areas on downwind outcomes. We are interested in two sets of parameter estimates. First, the coefficients on θ reveal the direct impact of upwind fires on downwind pollution and mortality. This serves as a useful benchmark, since fires are expected to worsen environmental outcomes. Second, we examine how the estimated forest coefficient β changes relative to estimates from equation (7), which does not control for fire activity. If the observed forest effect primarily reflects fire-driven pollution, then introducing fire controls should attenuate the β estimates accordingly.

5.3 Results

Figure 5 plots the β coefficients from equation (7). Each chart represents results for a separate outcome. Start with panel (a), which shows atmospheric outcomes. To facilitate interpretation and comparison of results, we use standardized outcomes (mean 0, standard deviation 1) in each regression, so that the interpretation of the β coefficients is "the number of standard deviation change in receiver city's atmospheric outcome per 1 standard deviation decrease in sender city's forest coverage."

The left panel of Figure 5a shows that forests have a large effect on downwind air pollution reduction. The middle and right panels of Figure 5a suggest there is little/null effect of upwind forests on downwind temperatures and precipitation. Two notable patterns are worth pointing out about the pollution effect. First, the forest-pollution effect increases monotonically with the downwind intensity score. In the strongest wind decile bin (bin "1st" on the x-axis), a standard deviation decrease in upwind forests increases downwind pollution concentrations by 3 standard deviations.[10] Second, we find precisely estimated zero effect for the no-wind bin (bin "calm" on the x-axis). This serves as a reassuring "placebo" exercise, suggesting that our econometric specification indicates an absence of forests' downstream environmental effect when our wind analysis indeed suggests an absence of a significant downwind relationship between the city pair. These two patterns (strong effects under high wind, and null effects under calm

[10] We will discuss plausibility of this effect size in conjunction with the health effects estimates.

wind) bolster a causal interpretation: they align exactly with the hypothesized mechanism that forest loss affects downwind pollution only when the atmospheric transport pathway is active.

The empirical impacts of forests on the atmospheric conditions is a subject of ongoing research. Here we compare our findings to some existing studies. On temperature effects, most empirical studies we are aware of document the *local* cooling effects of forests through shading and evapotranspiration (e.g., Han et al., 2021), and so it is not surprising we are not finding a transported effect at large-distance scale. The small negative coefficient in the strongest wind bin may reflect a mechanical effect of strong winds, which can enhance ventilation and slightly lower ambient temperatures. On precipitation effects, our null effects seem at odds with recent studies that show positive impacts of forests on downwind rainfalls (Grosset-Touba, Papp, and Taylor, 2023). One important difference of our estimation and Grosset-Touba, Papp, and Taylor (2023) is the time scale: while we look at monthly frequency impacts, their findings pertain mostly to longer-term changes. In Appendix Figure 7, we show that, when aggregating our analysis to the annual level, we do see a substantial positive impact of forests on downwind precipitation.[11] Our pollution results echo Xing et al. (2023) which uses a similar design – though looking at within-city scale – to examine the impact of urban forests on city air quality improvement.

We report health effect estimates in Figure 5b. Given the findings of forests' impact on air quality, we separately examine mortality due to cardiovascular/respiratory causes – which are expected to be more responsive to pollution changes – and other, non-cardiorespiratory causes. The left panel of Figure 5b shows that upwind forest losses lead to significant increase in downwind cardiorespiratory mortality rates. Once again, as we saw in the pollution analysis results, the mortality effects are monotonic with respect to downwind intensity score, and we find a precise-zero effect when there are no significant downwind connections between the city pair. The middle panel reports that we find little impact of upwind forests on mortality of non-cardiorespiratory causes. Finally, as an additional "placebo" exercise, in the right panel we look specifically at mortality due to external causes ("accidents") and we find no relationship between upwind forests and external mortality, regardless of downwind intensity levels.

[11] While forests can contribute to increased local humidity through evapotranspiration, this increased moisture might not be sufficient to alter weather patterns significantly in the downwind area, especially over short distances or periods. Over the long term, extensive forests can modify regional climate patterns. As forests mature, they contribute to higher levels of evapotranspiration. This increased moisture in the air can eventually influence weather patterns, potentially leading to more rainfall in downwind areas.

In Appendix Figure 9 we present a heterogeneity analysis in which we use land cover transition information to classify each upwind city-year's forest volume based on its land cover type from the previous year, distinguishing how much of the current year's forest acreage was previously forest, non-forest vegetation land, agricultural land, or non-vegetated land (i.e., urbanized area). We then separately estimate the impacts of upwind forests on downwind air quality and cardio-respiratory mortality based on the previous year's land cover. We found that environmental and health benefits primarily arise when upwind areas were forested in the previous year, as opposed to other land cover types. In other words, losing an area of intact natural forest has a much larger downwind pollution and health impact than losing an equivalent area of secondary vegetation or farmland. This result implies that mature forests provide larger pollution-filtering services, whereas recently planted forests or areas that were not forest to begin with do not confer the same protective benefit. This heterogeneity strengthens the case that it is the loss of natural forests (and the ecosystem functions they perform) that is driving the pollution and mortality increases.

Appendix Figure 10 presents tests on the role of upwind fire activity in mediating the effects of deforestation, based on estimation results from Equation (8). Panel (a) shows the direct effect of upwind fire activity on downwind pollution and cardio-respiratory mortality. We observe a clear increase in pollution levels following fire events, particularly in the highest wind deciles. While the estimated mortality effects exhibit a similar gradient, they are imprecisely estimated and not statistically distinguishable from zero. One potential explanation is that fire-induced pollution tends to be short-lived and episodic—producing sharp but brief spikes in air pollution—whereas mortality risk is more likely to reflect both short-term and sustained exposure. In our setting, pollution from deforestation (via the loss of forest filtering) likely alters background air quality more persistently, increasing the likelihood of a detectable mortality signal. Indeed, Panel (b) shows that our baseline forest effect estimates are virtually unchanged after controlling for upwind fire activity, across both pollution and mortality outcomes. Together, these findings suggest that the pollution-cleansing mechanism, rather than transient emissions from fires, is the dominant channel linking deforestation to downwind environmental and health harm in our setting.

The magnitude of our pollution and health estimates is also important to contextualize. At the strongest downwind wind exposure, a one standard deviation decrease in forest cover was

associated with roughly a 65 $\mu g/m^3$ rise in particulate matter (PM_{10}) concentration. The corresponding impact on the downwind cardiorespiratory mortality rate is on the order of +0.37 deaths per 100,000 people. This implies a pollution-mortality elasticity of about 1%, which is well within the range of estimates from prior literature. For example, Deryugina et al. (2019) find an elasticity of approximately 1.86% for PM2.5 and mortality among the elderly in the United States. Our estimate, encompassing the general population in Brazil, is somewhat smaller but of the same order of magnitude. This comparison suggests our results are plausible and perhaps even conservative relative to well-studied pollution-health relationships, lending credibility to the causal interpretation of the health impact.

6. Discussion and Conclusion

Aggregate Health Costs of Trade-Induced Deforestation. Bringing together our empirical estimates, we assess the aggregate health cost attributable to trade-induced deforestation in Brazil. We plug in various pieces of our empirical estimates back into the conceptual equation (1) we laid out in Section 3. The empirical version of the equation is as follows:

$$\text{Excess deaths due to city } i\text{'s agricultural trade deforestation} = \sum_{r,m,y} \left(\beta_{\Delta\text{Trade}\to\Delta\text{Forest}} \cdot \Delta\text{Trade}_i\right) \cdot \left(\beta^{i\to r,m,y}_{\text{Forest}\to\text{CR mortality}} \cdot \text{Population}_{r,y}\right) \quad (9)$$

That is, the total excess deaths due to city i equals the product of trade-induced deforestation in i (the first parenthesis) and excess deaths per unit of deforestation at a receiver city r (the second parenthesis), summed across all receiver cities and time periods. The subscript of the term $\beta^{i\to r,m,y}_{\text{Forest}\to\text{CR mortality}}$ means we only consider the impact of forest on downwind cardiovascular mortality – what we found to be responding to upwind forest changes; the superscript indicates we use nonlinear estimates as shown in Figure 5, panel (b) based on the downwind index associated with the city pair $i \to r$, month m, and year y.

One key qualitative insight from this calculation is that trade shocks (and the resulting deforestation) occur in areas distinct from where the associated mortality burden is felt. Figure 5, panel (a) shows a map of trade-induced deforestation based on our estimates. In panel (b), we plot the distribution of total mortality burdens at receiver cities. That is, for each city, we sum up

excess deaths due to deforestation from all upwind cities over the study period. The difference of the spatial patterns between the two panels is apparent: because of wind directivity and population distribution, areas with large numbers of excess deaths may situate hundreds if not thousands of miles away from where trade deforestation is happening.

Quantitatively, our estimates suggest a total of 3.6 million ha loss of Brazilian forests due to trade, resulting in over 732,000 excess deaths over the study period. For reference, total deaths in Brazil in the year of 2018 is estimated to be around 1.28 million. We quantify the mortality impacts in terms of its statistical life value, which is a common way to think about the costs (values) of environmental damage (protection) (e.g., U.S. EPA, 2000). Because direct estimation of the value of a statistical life (VSL) for Brazil is lacking, we use a transfer approach that downscales the U.S.-based VSL estimate of $2.3 million (Ashenfelter and Greenstone, 2004) by factors of a transfer elasticity of 1.2 (Narain and Sall, 2016) times a Brazil-U.S. income per capita ratio of 7. This yields a VSL estimate of $0.7 million USD. The total statistical life value loss of the 732,000 extra deaths thus amounts to about 513 billion USD. This represents a significant number – about 18 percent of the total agricultural export value of Brazil over the study period.

Our estimated elasticity of 0.18 may underestimate the actual health effects of trade-induced deforestation, as it does not account for morbidity, long-term health impacts beyond same-month pollution exposure, or productivity and income losses that could indirectly worsen health outcomes. In addition to air pollution, trade-induced deforestation may also degrade water quality, alter microclimates, and disrupt ecosystems, all of which could further affect health and increase the actual elasticity between agricultural exports and mortality.

Our study does not suggest that agricultural trade is inherently negative. Trade can generate multiplier effects in the exporting country through sectoral changes, employment, and migration, leading to welfare gains that exceed the value of the exports themselves. However, our paper highlights a large negative aspect of trade on health and the resulting regional inequality, as the mortality costs and income benefits may not be distributed in the same areas.

With increased globalization, to meet foreign demand without high health costs, agricultural producers should prioritize increasing yield rather than expanding agricultural lands. This requires domestic policies for deforestation monitoring, which are shown to be effective in our heterogeneity results across presidential administrations. International pressure or green

trade policy can also effectively avoid deforestation shown by existing studies (e.g. Nolte et al., 2013; Kerr, 2013; Hsiao, 2021).

Concluding Remarks. This study documents a sizeable and previously underappreciated cost of agricultural trade by establishing a causal link between export-driven deforestation and human mortality across distant locations. Our empirical findings highlight that the environmental impacts of globalization are not confined to local areas of resource extraction; they propagate through natural networks (like atmospheric flows) to affect populations far away. This insight expands our understanding of trade–environment interactions, showing that analyses of trade policy must account for spatially diffuse externalities and the unequal distribution of costs and benefits. Importantly, our results do not imply that trade liberalization or agricultural development is unwelcome; rather, they stress that sustainable development requires balancing growth with the stewardship of natural capital. The fact that even immediate health impacts of deforestation are sizable sends an important message that preserving forests is not only about long-run climate goals or ecosystem equilibrium, but also about saving lives today.

For future research, our paper provides a framework to estimate the value of forest and other natural capitals. Our identification strategy relies on foreign demand changes that serve as exogeneous drivers of forest loss, as well as quasi-random wind flow that separates upwind drivers and downwind recipients. For the latter, future studies may exploit other networks that connect spatially different regions. In addition, our wind trajectory simulation is also helpful for future environmental economics studies to estimate the impacts of air pollution.

References

Abman, Ryan, and Clark Lundberg. "Does free trade increase deforestation? The effects of regional trade agreements." **Journal of the Association of Environmental and Resource Economists** 7.1 (2020): 35-72.

Adda, Jérôme, and Yarine Fawaz. "The health toll of import competition." **The Economic Journal** 130, no. 630 (2020): 1501-1540.

Adão, Rodrigo, Kolesár, Michal and Morales, Eduardo, (2019), Shift-Share Designs: Theory and Inference, **The Quarterly Journal of Economics**, 134, issue 4, p. 1949-2010.

Aerts, Raf, and Olivier Honnay. "Forest restoration, biodiversity and ecosystem functioning." **BMC Eology** 11 (2011): 1-10.

Alcalá, Francisco, and Antonio Ciccone. "Trade and productivity." **The Quarterly Journal of Economics 119**, no. 2 (2004): 613-646.

Andela, Niels, Douglas C. Morton, Louis Giglio, Yang Chen, Guido R. van der Werf, Prasad S. Kasibhatla, Rurth S. DeFries et al. "A human-driven decline in global burned area." **Science** 356, no. 6345 (2017): 1356-1362.

Anderson, Michael L. "Multiple inference and gender differences in the effects of early intervention: A reevaluation of the Abecedarian, Perry Preschool, and Early Training Projects." **Journal of the American Statistical Association** 103, no. 484 (2008): 1481-1495.

Anderson, Michael L. "As the wind blows: The effects of long-term exposure to air pollution on mortality." **Journal of the European Economic Association** 18, no. 4 (2020): 1886-1927.

Antweiler, Werner, Brian R. Copeland, and M. Scott Taylor. "Is free trade good for the environment?" **American Economic Review** 91, no. 4 (2001): 877-908.

Ashenfelter, Orley, and Michael Greenstone. "Using mandated speed limits to measure the value of a statistical life." **Journal of Political Economy** 112, no. S1 (2004): S226-S267.

Assunção, Juliano, Clarissa Gandour, Romero Rocha, and Rudi Rocha. "The effect of rural credit on deforestation: evidence from the Brazilian Amazon." **The Economic Journal** 130, no. 626 (2020): 290-330.

Balboni, Clare, Aaron Berman, Robin Burgess, and Benjamin A. Olken. "The economics of tropical deforestation." **Annual Review of Economics** 15 (2023): 723-754.

Barona, Elizabeth, Navin Ramankutty, Glenn Hyman, and Oliver T. Coomes. "The role of pasture and soybean in deforestation of the Brazilian Amazon." **Environmental Research Letters** 5, no. 2 (2010): 024002.

Berazneva, Julia, and Tanya S. Byker. "Does forest loss increase human disease? Evidence from Nigeria." **American Economic Review** 107, no. 5 (2017): 516-521.

Berazneva, Julia, and Tanya S. Byker. "Impacts of Environmental Degradation: Forest, Loss, Malaria, and Child Outcomes in Nigeria." **Review of Economics and Statistics** (2022): 1-46.

Betts, Richard, Michael Sanderson, and Stephanie Woodward. "Effects of large-scale Amazon forest degradation on climate and air quality through fluxes of carbon dioxide, water, energy, mineral dust and isoprene." **Philosophical Transactions of the Royal Society B: Biological Sciences** 363.1498 (2008): 1873-1880.

Bombardini, Matilde, and Bingjing Li. "Trade, pollution and mortality in China." **Journal of International Economics** 125 (2020): 103321.

Bonan, Gordon B. "Forests and climate change: forcings, feedbacks, and the climate benefits of forests." **Science** 320, no. 5882 (2008): 1444-1449.

Borgschulte, Mark, David Molitor, and Eric Yongchen Zou. "Air pollution and the labor market: Evidence from wildfire smoke." **Review of Economics and Statistics** (2022): 1-46.

Borusyak, Kirill, Peter Hull, and Xavier Jaravel. "Quasi-experimental shift-share research designs." **The Review of Economic Studies** 89, no. 1 (2022): 181-213.

Brazil, W. W. F. "Brazil's new Forest Code: A guide for decision-makers in supply chains and governments." (2016).

Bryan, Brett A., Lei Gao, Yanqiong Ye, Xiufeng Sun, Jeffery D. Connor, Neville D. Crossman, Mark Stafford-Smith et al. "China's response to a national land-system sustainability emergency." **Nature** 559, no. 7713 (2018): 193-204.

Busch, Jonah, and Kalifi Ferretti-Gallon. "What drives deforestation and what stops it? A meta-analysis." **Review of Environmental Economics and Policy** (2017).

Carreira, Igor, Francisco Costa, and Joao Paulo Pessoa. "The deforestation effects of trade and agricultural productivity in Brazil." **Journal of Development Economics** 167 (2024): 103217.

Coates, Jane, Kathleen A. Mar, Narendra Ojha, and Tim M. Butler. "The influence of temperature on ozone production under varying NOx conditions – a modelling study." **Atmospheric Chemistry and Physics 16**, no. 18 (2016): 11601-11615.

Copeland, Brian R., Joseph S. Shapiro, and M. Scott Taylor. Globalization and the Environment. No. w28797. **National Bureau of Economic Research**, 2021.

Curtis, Philip G., Christy M. Slay, Nancy L. Harris, Alexandra Tyukavina, and Matthew C. Hansen. "Classifying drivers of global forest loss." **Science** 361, no. 6407 (2018): 1108-1111.

Dasgupta, Partha. **The Economics of Biodiversity: the Dasgupta Review**. Hm Treasury, 2021.

Davis, Steven J., and John Haltiwanger. "Gross job creation, gross job destruction, and employment reallocation." **The Quarterly Journal of Economics** 107, no. 3 (1992): 819-863.

Deryugina, Tatyana, Garth Heutel, Nolan H. Miller, David Molitor, and Julian Reif. "The mortality and medical costs of air pollution: Evidence from changes in wind direction." **American Economic Review** 109, no. 12 (2019): 4178-4219.

Ebenstein, Avraham, Maoyong Fan, Michael Greenstone, Guojun He, and Maigeng Zhou. "New evidence on the impact of sustained exposure to air pollution on life expectancy from China's Huai River Policy." **Proceedings of the National Academy of Sciences** 114, no. 39 (2017): 10384-10389.

Ehrl, Philipp., 2017. Minimum comparable areas for the period 1872-2010: an aggregation of Brazilian municipalities. Estudos Econômicos (São Paulo), 47, pp.215-229.

Farrokhi, Farid, Elliot Kang, Heitor S. Pellegrina, and Sebastian Sotelo. "Deforestation: A global and dynamic perspective." (2023). Working paper.

Fearnside, Philip M. "Deforestation in Brazilian Amazonia: history, rates, and consequences." **Conservation Biology** 19, no. 3 (2005): 680-688.

Ferreira, Susana. "Deforestation, property rights, and international trade." **Land Economics** 80, no. 2 (2004): 174-193.

Frank, Eyal G., and Wolfram Schlenker. "Balancing economic and ecological goals." **Science** 353, no. 6300 (2016): 651-652.

Frankel, Jeffrey A., and Andrew K. Rose. "Is trade good or bad for the environment? Sorting out the causality." **Review of Economics and Statistics** 87.1 (2005): 85-91.

Franklin Jr, Sergio L., and Robert S. Pindyck. "Tropical forests, tipping points, and the social cost of deforestation." **Ecological Economics** 153 (2018): 161-171.

Garg, Teevrat. "Ecosystems and human health: The local benefits of forest cover in Indonesia." **Journal of Environmental Economics and Management** 98 (2019): 102271.

Gong, Yazhen, Shanjun Li, Nicholas J. Sanders, and Guang Shi. "The mortality impact of fine particulate matter in China: Evidence from trade shocks." **Journal of Environmental Economics and Management** 117 (2023): 102759.

Graff Zivin, Joshua, and Matthew Neidell. "The impact of pollution on worker productivity." **American Economic Review** 102, no. 7 (2012): 3652-3673.

Graff Zivin, Joshua, Matthew Neidell, Nicholas J. Sanders, and Gregor Singer. "When externalities collide: Influenza and pollution." **American Economic Journal: Applied Economics** 15, no. 2 (2023): 320-351.

Grosset-Touba, Florian, Anna Papp, and Charles Taylor. "Rain follows the forest: Land use policy, climate change, and adaptation." **Climate Change, and Adaptation** (December 1, 2023) (2023).

Grossman, Gene M., and Elhanan Helpman. "Trade, innovation, and growth." **The American Economic Review** 80.2 (1990): 86-91.

Guerrico, Sofía Fernández. "The effects of trade-induced worker displacement on health and mortality in Mexico." **Journal of Health Economics** 80 (2021): 102538.

Guidetti, Bruna, Paula Pereda, and Edson R. Severnini. Health shocks under hospital capacity constraint: Evidence from air pollution in sao paulo, brazil. No. w32224. **National Bureau of Economic Research**, 2024.

Han, Lu, Stephan Heblich, Christopher Timmins, and Yanos Zylberberg. Cool cities: The value of urban trees. No. w32063. **National Bureau of Economic Research**, 2024.

Harstad, Bård. "Trade and trees." **American Economic Review: Insights** 6, no. 2 (2024): 155-175.

Heilmayr, Robert, Lisa L. Rausch, Jacob Munger, and Holly K. Gibbs. "Brazil's Amazon soy moratorium reduced deforestation." **Nature Food** 1, no. 12 (2020): 801-810.

Heo, Seonmin Will, Koichiro Ito, and Rao Kotamarthi. International spillover effects of air pollution: evidence from mortality and health data. No. w30830. **National Bureau of Economic Research**, 2023.

Hsiao, Allan. "Coordination and commitment in international climate action: evidence from palm oil." Unpublished, Department of Economics, MIT (2021).

Jayachandran, Seema, Joost De Laat, Eric F. Lambin, Charlotte Y. Stanton, Robin Audy, and Nancy E. Thomas. "Cash for carbon: A randomized trial of payments for ecosystem services to reduce deforestation." **Science** 357, no. 6348 (2017): 267-273.

Jones, Benjamin A., and Andrew L. Goodkind. "Urban afforestation and infant health: Evidence from MillionTreesNYC." **Journal of Environmental Economics and Management** 95 (2019): 26-44.

Kerr, Suzi C. "The economics of international policy agreements to reduce emissions from deforestation and degradation." **Review of Environmental Economics and Policy** (2013).

Levchenko, Andrei A. "Institutional quality and international trade." **The Review of Economic Studies** 74.3 (2007): 791-819.

Lewinsohn, Thomas M., and Paulo Inácio Prado. "How many species are there in Brazil?." **Conservation Biology** 19, no. 3 (2005): 619-624.

Li, Liqing. "Environmental goods provision and gentrification: Evidence from MillionTreesNYC." **Journal of Environmental Economics and Management** 120 (2023): 102828.

Managi, Shunsuke, Akira Hibiki, and Tetsuya Tsurumi. "Does trade openness improve environmental quality?" **Journal of Environmental Economics and Management** 58.3 (2009): 346-363.

Mullan, Katrina, Trent Biggs, Jill Caviglia-Harris, Jime Rodrigues Ribeiro, T. Ottoni, Erin Sills, and T. A. West. "Estimating the value of NearReal-time satellite information for monitoring deforestation in the Brazilian Amazon." Resources for the Future (2022).

Narain, Urvashi, and Chris Sall. "Methodology for valuing the health impacts of air pollution: discussion of challenges and proposed solutions." (2016).

Nolte, Christoph, Arun Agrawal, Kirsten M. Silvius, and Britaldo S. Soares-Filho. "Governance regime and location influence avoided deforestation success of protected areas in the Brazilian Amazon." **Proceedings of the National Academy of Sciences** 110, no. 13 (2013): 4956-4961.

Nunes, Felipe SM, Britaldo S. Soares-Filho, Amanda R. Oliveira, Laura VS Veloso, Jair Schmitt, Richard Van der Hoff, Debora C. Assis et al. "Lessons from the historical dynamics of environmental law enforcement in the Brazilian Amazon." **Scientific Reports** 14, no. 1 (2024): 1828.

Pan, Yude, Richard A. Birdsey, Jingyun Fang, Richard Houghton, Pekka E. Kauppi, Werner A. Kurz, Oliver L. Phillips et al. "A large and persistent carbon sink in the world's forests." **Science** 333, no. 6045 (2011): 988-993.

Pendrill, Florence, Toby A. Gardner, Patrick Meyfroidt, U. Martin Persson, Justin Adams, Tasso Azevedo, Mairon G. Bastos Lima et al. "Disentangling the numbers behind agriculture-driven tropical deforestation." **Science** 377, no. 6611 (2022): eabm9267.

Phillips, Benjamin B., James M. Bullock, Juliet L. Osborne, and Kevin J. Gaston. "Spatial extent of road pollution: A national analysis." **Science of the Total Environment** 773 (2021): 145589.

Pierce, Justin R., and Peter K. Schott. "Trade liberalization and mortality: evidence from US counties." **American Economic Review: Insights** 2, no. 1 (2020): 47-63.

Rangel, Marcos A., and Tom S. Vogl. "Agricultural fires and health at birth." **Review of Economics and Statistics** 101, no. 4 (2019): 616-630.

Song, Xiao-Peng, Matthew C. Hansen, Peter Potapov, Bernard Adusei, Jeffrey Pickering, Marcos Adami, Andre Lima et al. "Massive soybean expansion in South America since 2000 and implications for conservation." **Nature Sustainability** 4, no. 9 (2021): 784-792.

Tanaka, Shinsuke, Kensuke Teshima, and Eric Verhoogen. "North-South displacement effects of environmental regulation: The case of battery recycling." **American Economic Review: Insights** 4, no. 3 (2022): 271-288.

UN Department of Economics of Social Affairs. "The Global Forest Goals Report 2021." United Nations Publication (2021).

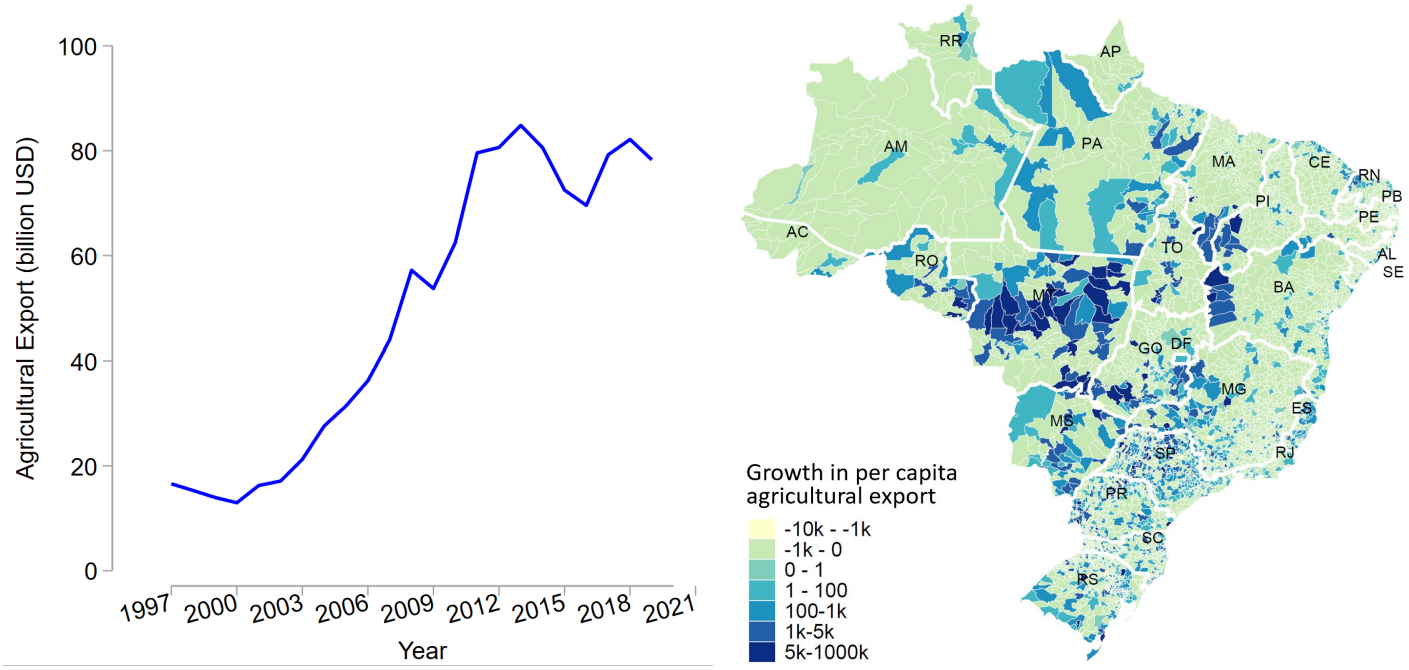
U.S. Environmental Protection Agency. "*Guidelines for Preparing Economic Analyses*." EPA 240-R-00-003 (2000).

Wei, Xiangying, Shiheng Lyu, Ying Yu, Zonghua Wang, Hong Liu, Dongming Pan, and Jianjun Chen. "Phylloremediation of air pollutants: exploiting the potential of plant leaves and leaf-associated microbes." **Frontiers in Plant Science** 8 (2017): 270745.

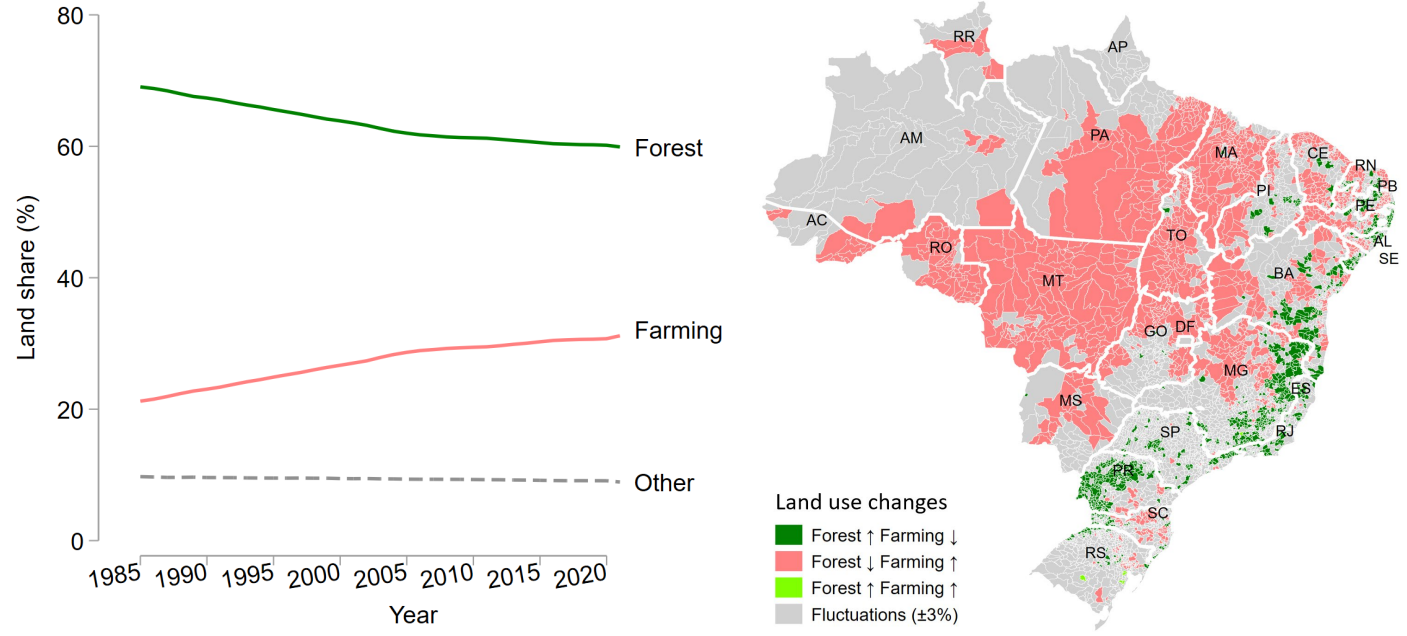
Xing, Jianwei, Zhiren Hu, Fan Xia, Jintao Xu, and Eric Zou. Urban Forests: Environmental Health Values and Risks. No. w31554. **National Bureau of Economic Research**, 2023.

Figure 1. Trends in Trade, Agricultural Expansion and Deforestation

(a) Agricultural Exports

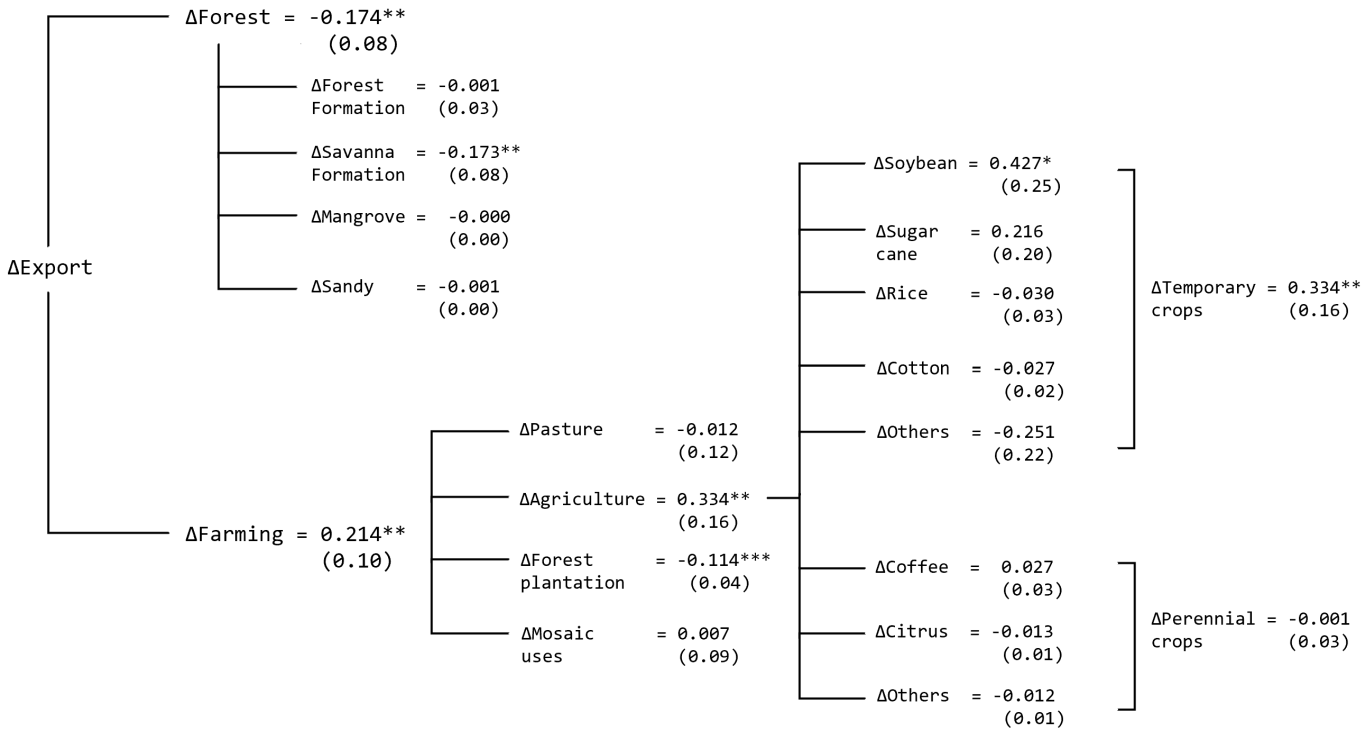


(b) Agricultural Land Expansion and Deforestation



Notes: Panel (a) shows temporal and geographic trends in Brazil's agricultural exports. Panel (b) shows temporal and geographic trends in the substitution between agricultural land and forests. "Fluctuations" correspond to areas with less than 3 percent changes in forest or farmland coverage over the study period.

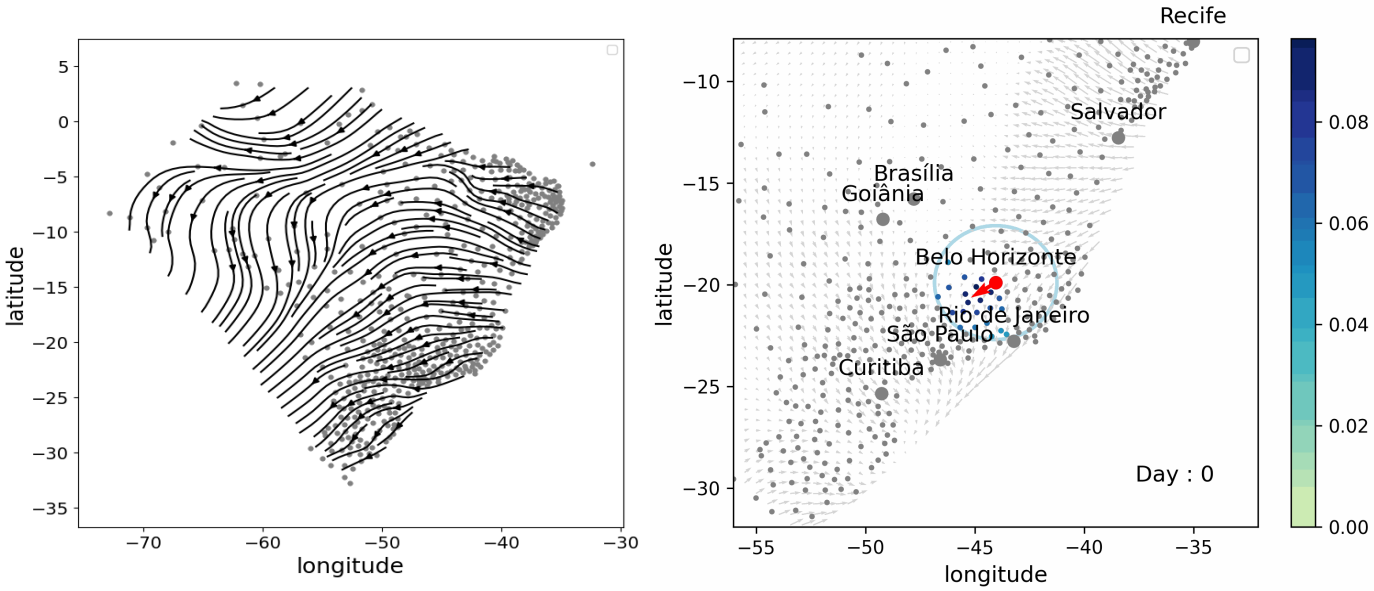
Figure 2. The Effect of Trade on Deforestation and Agricultural Expansion



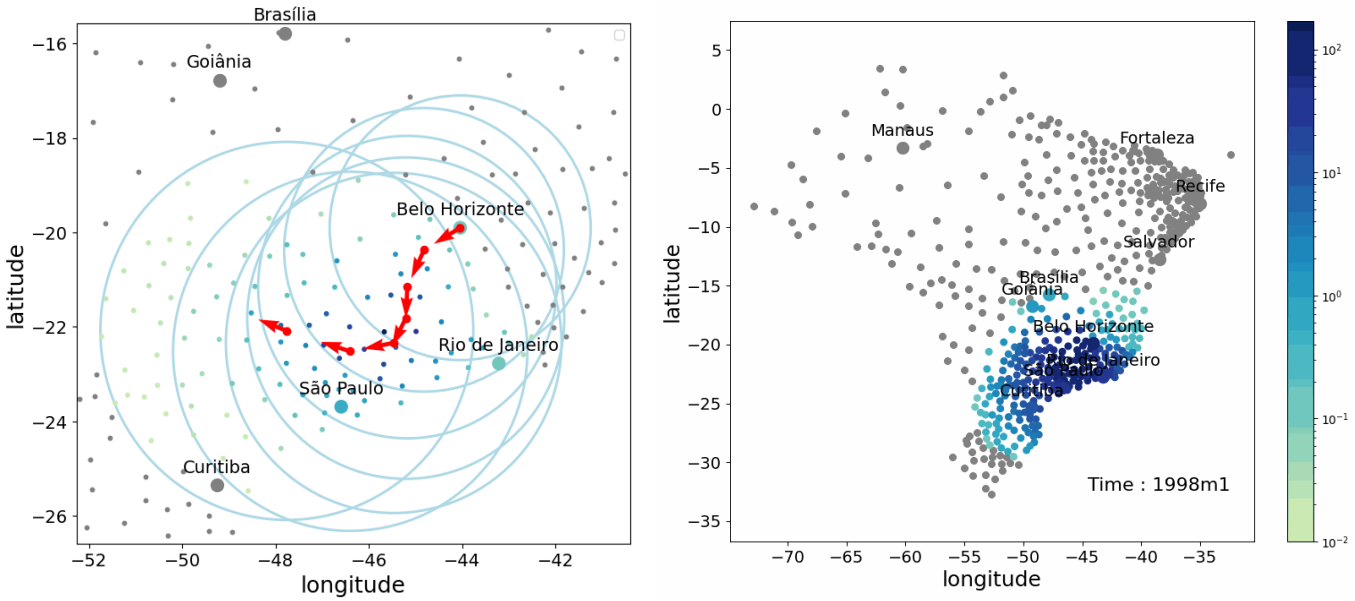
Notes: Each node on the tree represents a separate IV regression following the exact same specification except for the outcome variable, which is denoted by the name of the node. Each regression has 57,189 underlying observations with a first-stage Kleibergen-Paap F-statistic of 8.1. Branches of the tree represent hierarchies of the land use categorizations. Interpretation of the coefficients is change in land cover land use type (in percentage points) per 1,000 BRL increase in export per capita.

Figure 3. Area-of-Effect Modeling

(a) Airflow Modeling

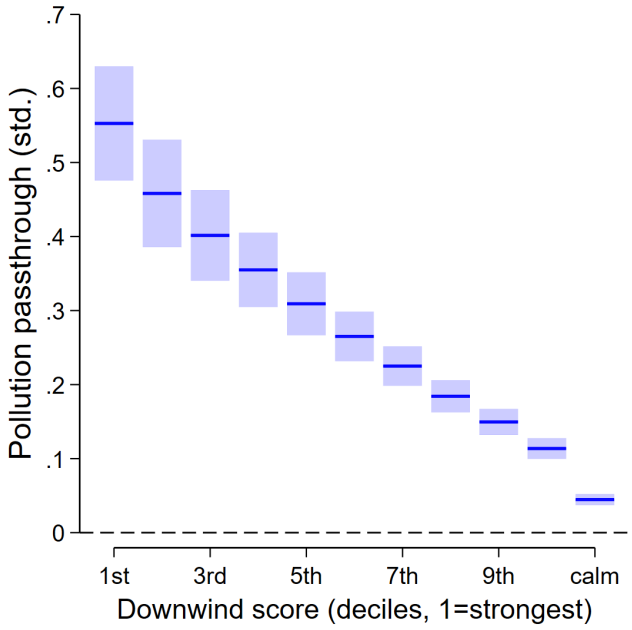


(b) Downwind Score: Belo Horizonte as Example



Notes: Figures show dotted map of Brazil where each dot represents centroid of a city. Panel (a) shows a day snapshot of wind flows built from location-specific wind vectors data (left) and a visualization of our wind flow model that tracks downwind cities influenced by winds from a sender city (Belo Horizonte in this example) over the course of seven steps (i.e., days). Panel (b) shows aggregation of step-specific downwind scores to sender-receiver-day level (left) and sender-receiver-month level (right) where the sender city is Belo Horizonte.

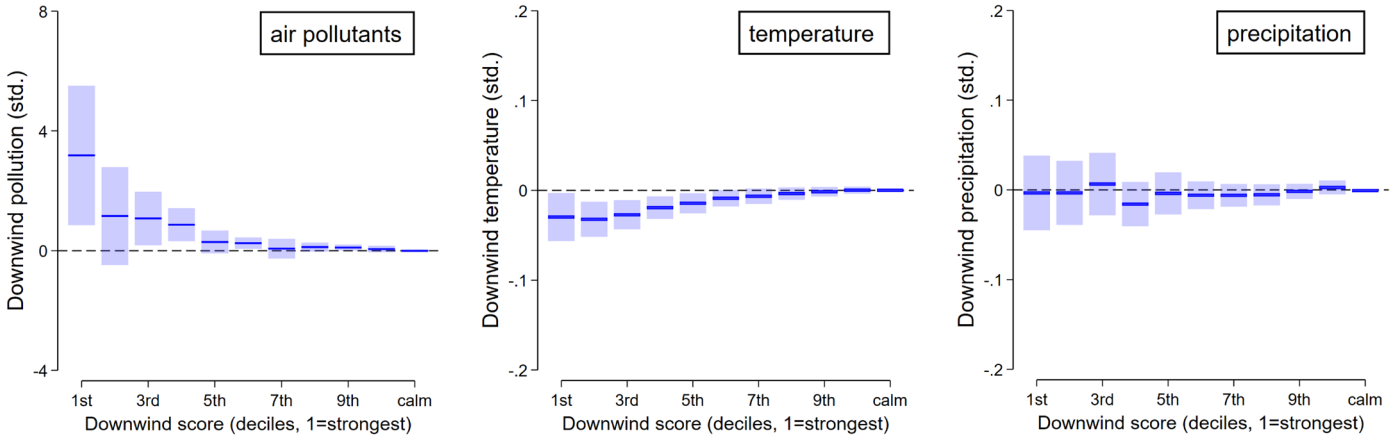
Figure 4. Validation Test of Air Pollution Passthrough from Upwind to Downwind Cities by Downwind Score Deciles



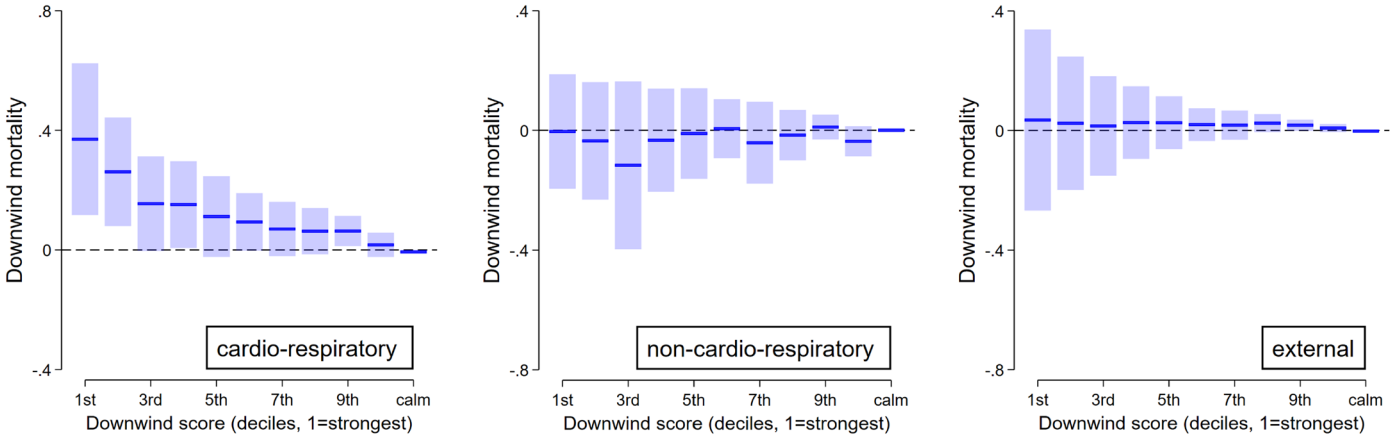
Notes: This figure shows coefficients from a regression of a receiver city's PM2.5 concentration on an upwind city's PM2.5 concentration, with the effect allowed to vary by the downwind score from the upwind location to the downwind location according to our area-of-effect model. All regression controls for city pair by month-of-sample fixed effects and year fixed effects. Standard errors are two-way clustered at the sender city and receiver city levels. Range bars show 95 percent confidence intervals.

Figure 5. The Downwind Effects of Forest Losses

(a) Atmospheric Outcomes

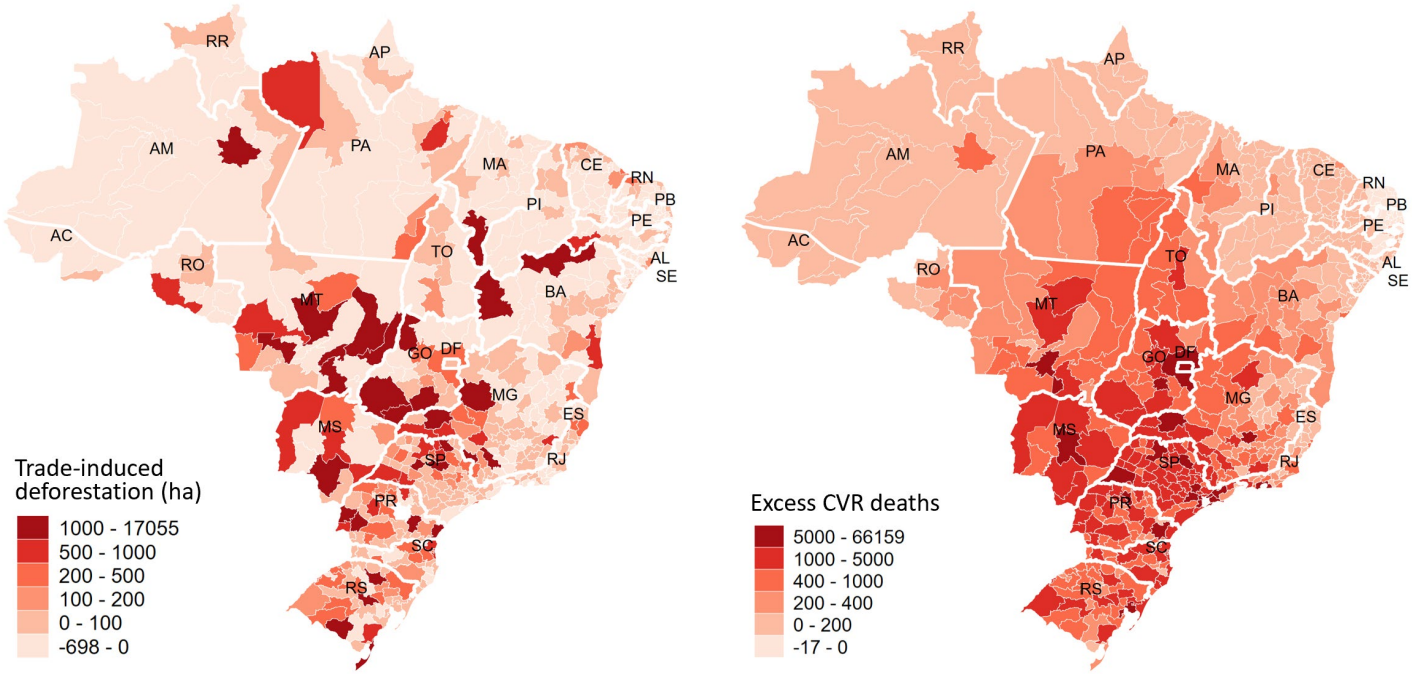


(b) Mortality Outcomes



Notes: Charts show estimates on changes in downwind outcomes per 1 SD decrease in upwind forest cover, separately by downwind exposure score bins. Each chart shows a separate regression following the exact same specification except for the outcome variable. Within each chart, horizontal step lines show point estimates, and range bars show 95 percent confidence intervals.

Figure 6. Distribution of Trade-Induced Forest Losses and Excess Deaths



Notes: The map on the left shows the spatial distribution of trade-induced deforestation over the study period. The map on the right shows the spatial distribution of the downstream cardio-respiratory deaths due to trade-induced deforestation.

Table 1. Summary Statistics

Variable Name	Obs	Mean	SD
ΔForest land share (%)	57189	-0.14	1.802
| ΔForest formation (%)	57189	0.04	0.994
| ΔSavanna formation (%)	57189	-0.18	1.488
| ΔMangrove (%)	57189	0.00	0.041
| ΔSandy (%)	57189	0.00	0.070
ΔFarming land share (%)	57189	0.08	1.990
| ΔPasture (%)	57189	-1.08	3.919
| ΔAgriculture (%)	57189	1.00	2.827
| | ΔSoybean (%)	57189	0.51	2.629
| | ΔSugar cane (%)	57189	0.60	2.710
| | ΔRice (%)	57189	0.01	0.467
| | ΔCotton (%)	57189	0.00	0.051
| | ΔCoffee (%)	57189	0.05	0.419
| | ΔCitrus (%)	57189	0.01	0.176
ΔForest plantation (%)	57189	0.26	0.730
ΔMosaic of uses (%)	57189	-0.10	2.764
ΔExport per capita (real 1000 BRL)	57189	0.19	1.562
Population	57189	48431.26	2.45e5
Agricultural employee	57189	23721.17	1.82e5
Income per capita	57189	191.40	114.516
Literacy rate (%)	57189	70.32	16.445
Population density	57189	0.82	3.808
Rural population	57189	9398.84	16462.78
Urban population	57189	28374.83	1.99e5
GE soy	57189	0.03	0.005

Notes: The variables for land use and export per capita describe the growth over four years within the period from 2001 to 2019; Real export values have been deflated by the Brazilian Consumer Price Index (IPCA) calculated by IBGE and are denominated in 2019 reals; Income per capita, literacy rate, population density, rural population, and urban population are values from 1991, calculated by IBGE.

Table 2. Shift-Share Balancing Tests

	(1) Coef.	(2) S.E.	(3) *p* value	(4) *q* value
Urban population	4704.262	3952.672	0.234	.429
Rural population	3050.763	2608.679	0.242	.429
Total population	7755.025	6395.578	0.225	.429
Per capita income	4.635	1.635	0.005	.060
Literacy rate	0.264	0.151	0.081	.429
Population density	-0.003	0.007	0.691	.754
GE soy seeds	0.000	0.000	0.608	.730
Average temperature	0.030	0.031	0.332	.498
Average humidity	-0.005	0.078	0.947	.947
Average pressure	-0.478	0.416	0.250	.429
Average wind speed	-0.006	0.007	0.383	.511
Total precipitation	652.890	438.455	0.137	.429

Notes: Export values are deflated by the Brazilian Consumer Price Index (IPCA) calculated by IBGE and are denominated in 2019 reais. The number of AMC regions is 3812. All regressions include Year fixed effects and macroregion fixed effects. The independent variable is the four-year shift-share instrument generated for the growth of Brazilian agricultural exports. "*q* value" is the False Discovery Rate adjusted significance level (Anderson, 2008)

Table 3. Trade-Deforestation Regression Estimates: Alternative Time Lags

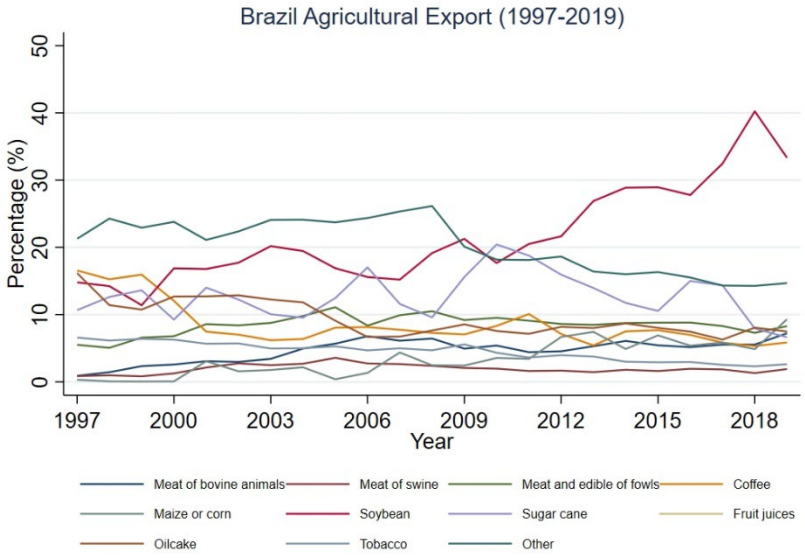
	(1)	(2)	(3)	(4)	(5)	(6)
Panel A. First stage	Export (Δ1y)	Export (Δ2y)	Export (Δ3y)	Export (Δ4y)	Export (Δ5y)	Export (Δ6y)
Shift-share IV	0.21	1.12***	1.78***	0.91***	1.12***	1.04***
	(0.14)	(0.12)	(0.30)	(0.23)	(0.25)	(0.28)
Panel B. Second stage	Forest (Δ1y)	Forest (Δ2y)	Forest (Δ3y)	Forest (Δ4y)	Forest (Δ5y)	Forest (Δ6y)
ΔExport per capita (1000 BRL)	-0.118	-0.038**	-0.043*	-0.174**	-0.207***	-0.192**
	(0.12)	(0.02)	(0.02)	(0.08)	(0.07)	(0.10)
Observations	68,585	68,585	64,814	57,189	49,564	41,939
First-stage F (Kleibergen-Paap)	1.25	81.63	41.01	8.07	16.59	6.49
Year FE	Yes	Yes	Yes	Yes	Yes	Yes
Macroregion FE	Yes	Yes	Yes	Yes	Yes	Yes
Control	Yes	Yes	Yes	Yes	Yes	Yes

Notes: The IVs are constructed based on the agricultural imports by top import countries. All monetary values have been deflated by the Brazilian Consumer Price Index (IPCA) calculated by IBGE and are denominated in 2019 reals. *: $p < 0.10$; **: $p < 0.05$; ***: $p < 0.01$.

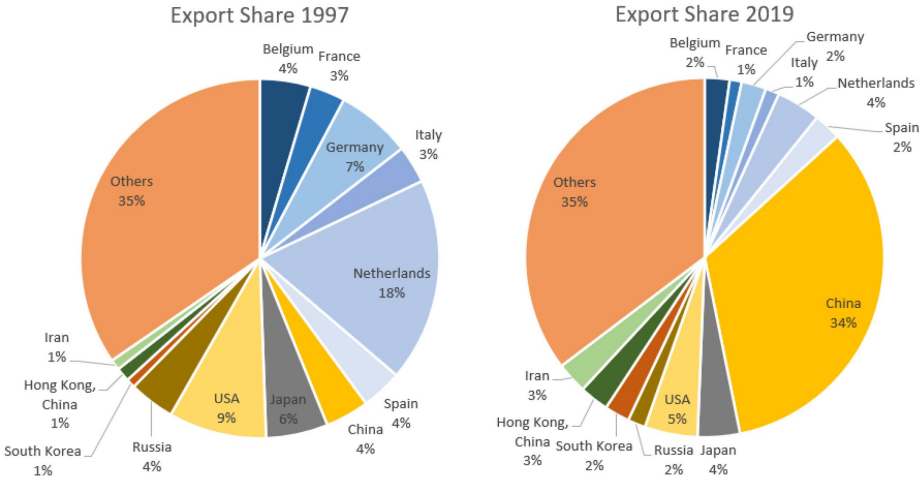
Appendix Figures and Tables

Appendix Figure 1. Brazil's Agricultural Export Structure

(a) Product Categories

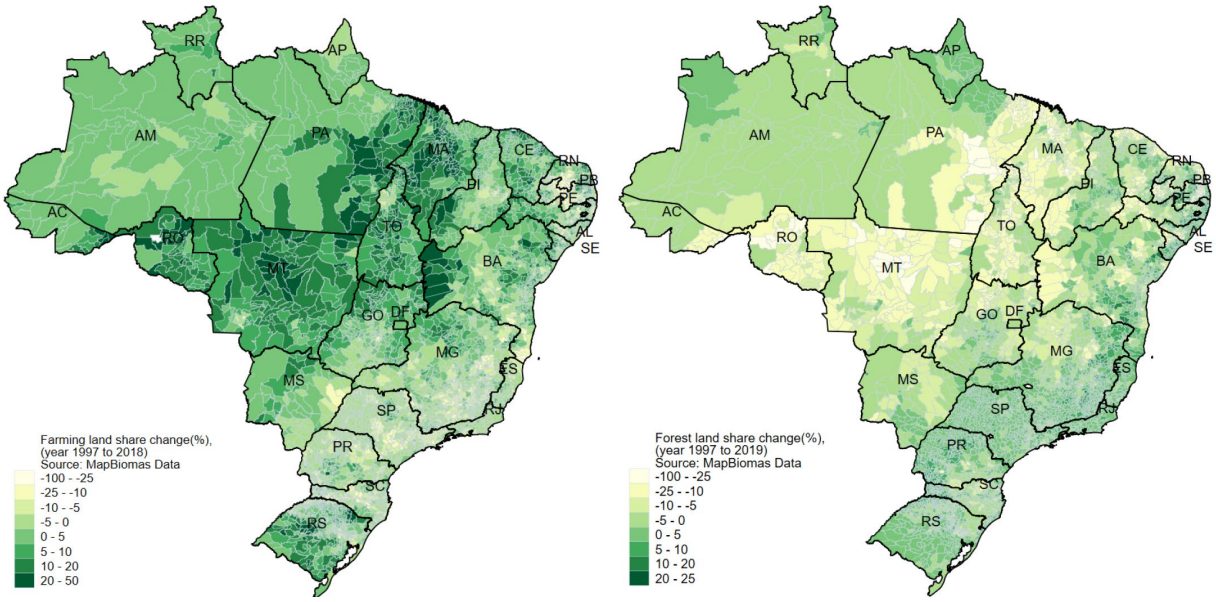


(b) Trade Partners



Notes: Panel (a) shows distribution of export values in billions of USD by product category. Panel (b) shows agricultural export share by trade partner in 1997 (left) and in 2019 (right).

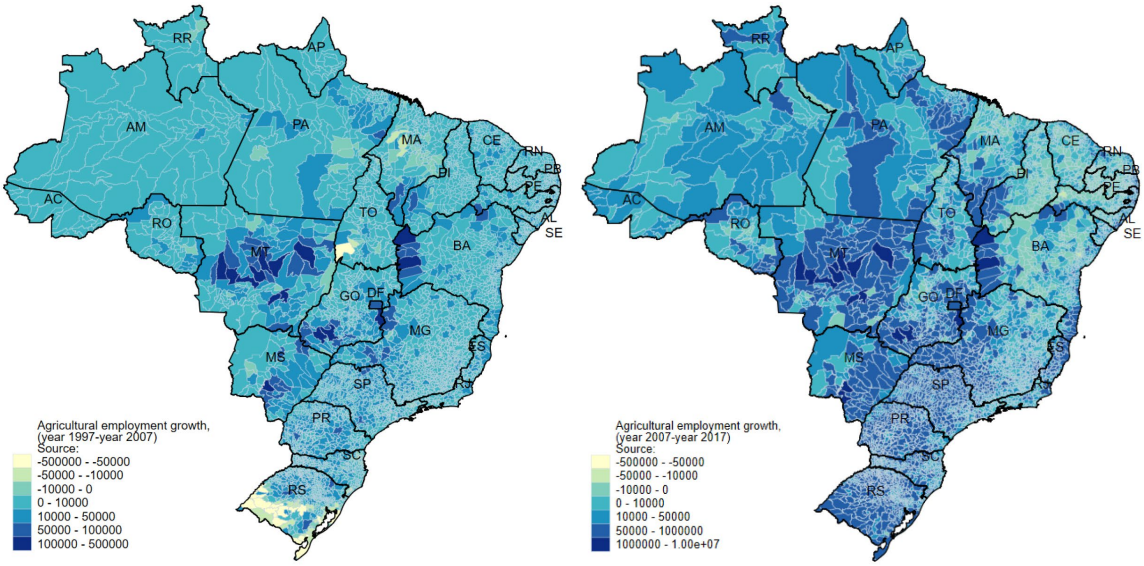
Appendix Figure 2. Geography of Land Use Changes



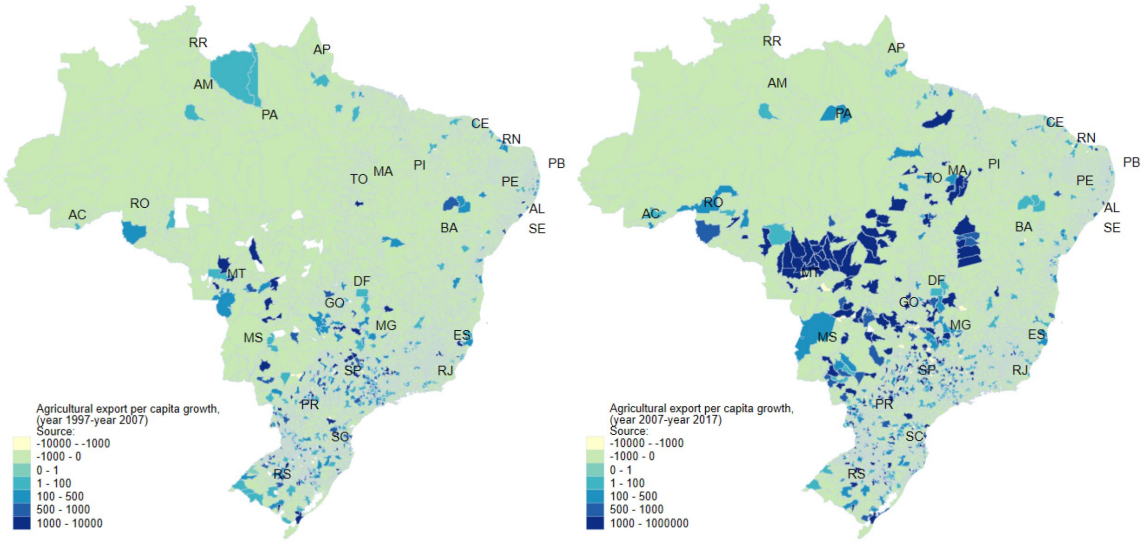
Notes: Maps show 1997-2018 percentage change in land use for farming purposes (left) and forest land (right).

Appendix Figure 3. Geography of Agricultural Growth

(a) Agricultural Employment Growth

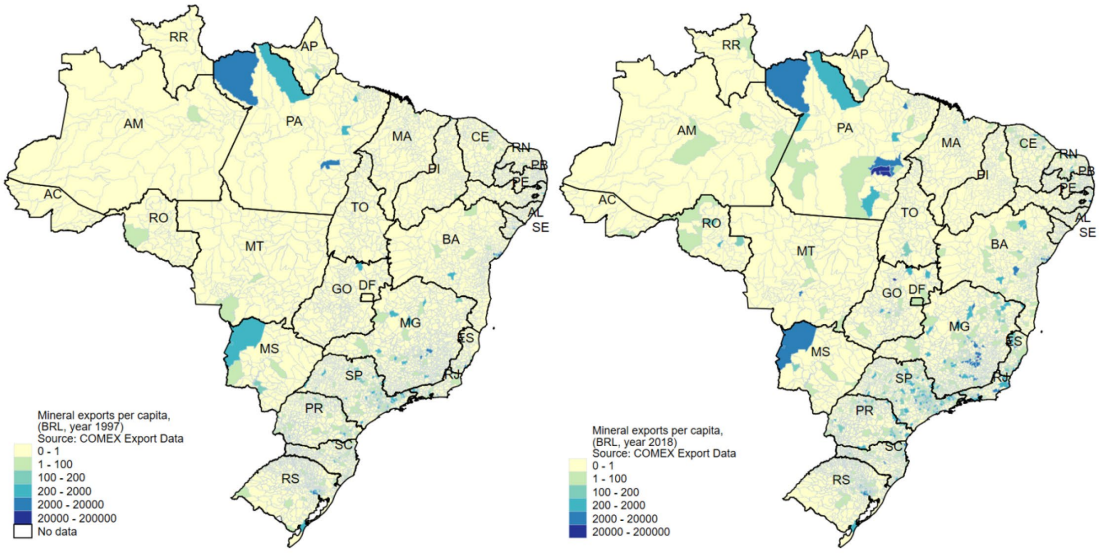


(b) Agricultural Export Growth



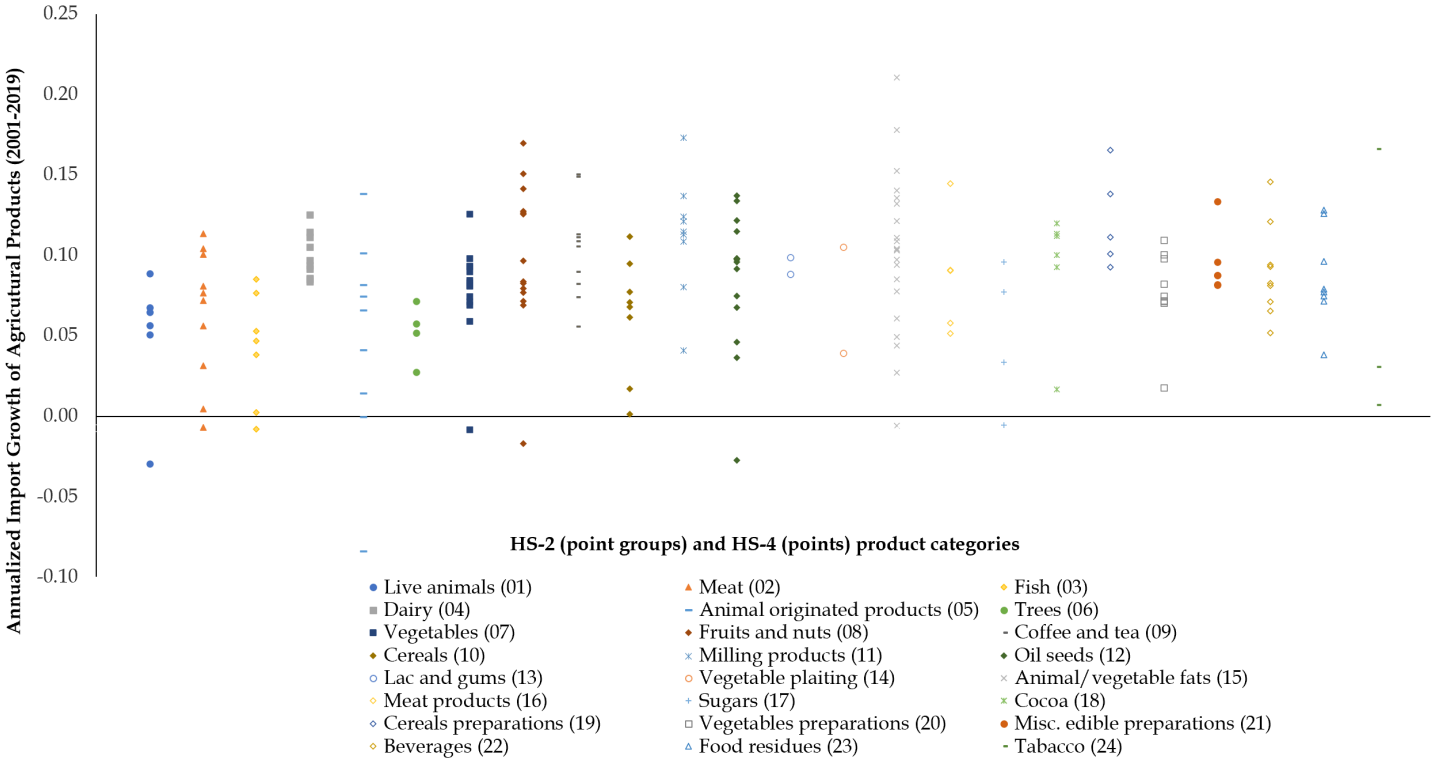
Notes: Panel (a) shows growth in agricultural employment over the 1997-2007 period (left) and the 2007-2019 period (right). Panel (b) shows growth in agricultural exports per capita over the 1997-2007 period (left) and the 2007-2019 period (right).

Appendix Figure 4. Geography of Mining Activities



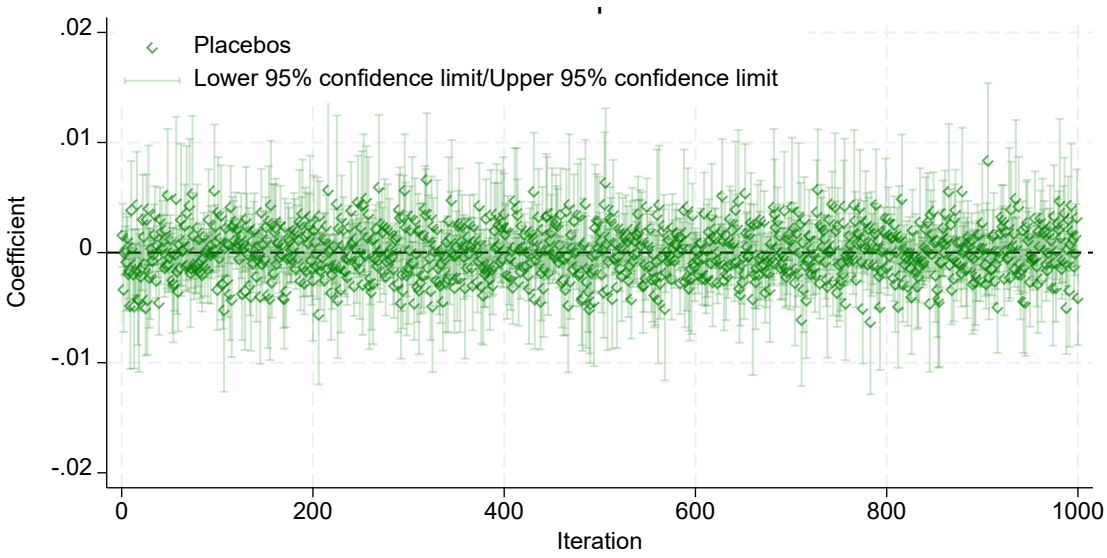
Notes: Maps show mineral exports per capita in year 1997 (left) and in year 2018 (right).

Appendix Figure 5. Export Demand Shock Variability



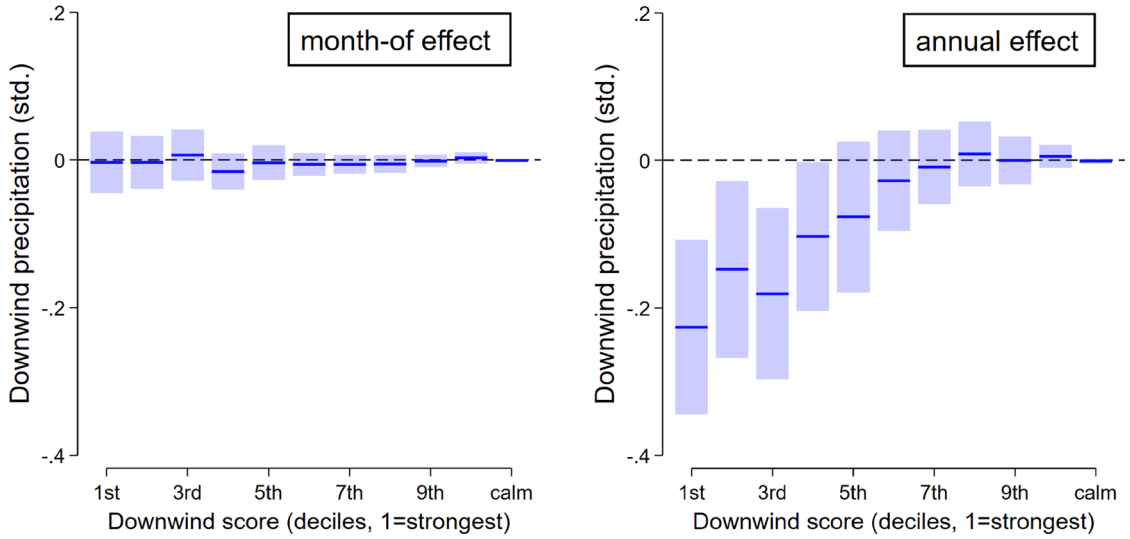
Notes: Major importing countries' export demand growth rates variation across HS-4 product categories, represented by points. Points are grouped into broader HS-2 categories.

Appendix Figure 6. Effects of Placebo Export Shocks on Forest Cover



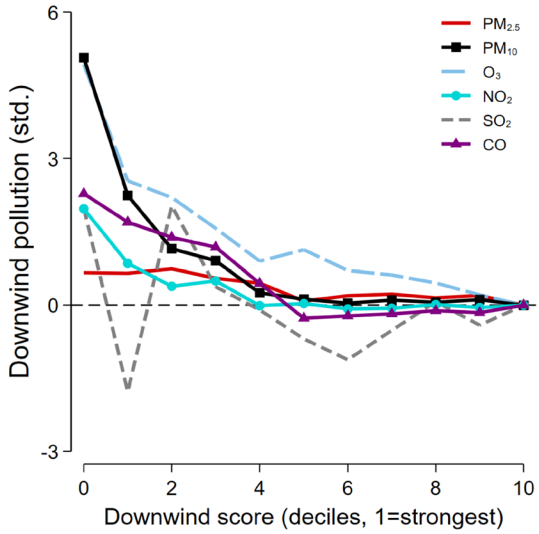
Notes: This figure plots the coefficient on placebo shocks in 1,000 separate regressions, where the dependent variable is the forest land use 4 years growth. The placebo shock is the placebo change in agricultural import growth by HS code and municipality, a normally distributed random variable with mean 0 and variance 5. The regression also contains year and macroregion fixed effects, and agricultural employees are used as weights. Standard errors are clustered at the AMC level.

Appendix Figure 7. The Downwind Effect of Forest Losses on Precipitation: Month-Of versus Annual Effects



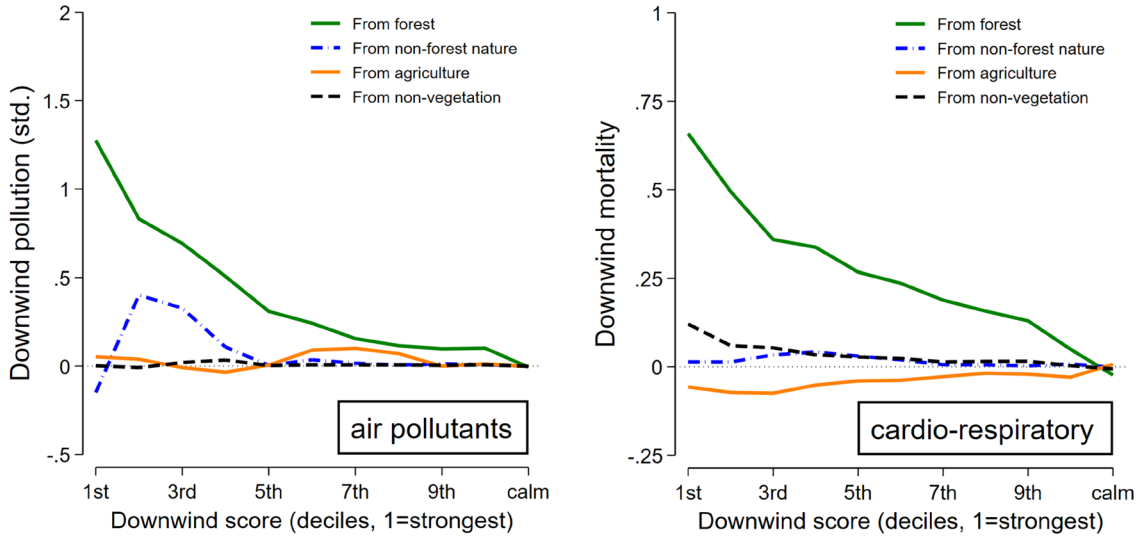
Notes: Charts show estimates on changes in downwind precipitation outcomes per 1 SD decrease in upwind forest cover. Left panel shows regression estimates based on monthly data. Right panel shows regression estimates from the same data aggregated to the annual level. The annual regression equation, analogous to the monthly equation (7), controls for sender-by-receiver fixed effects and year fixed effects, with standard errors two-way clustered at the sender and receiver levels.

Appendix Figure 8. The Downwind Effect of Forest Losses on Air Pollutants



Notes: Chart shows estimates on changes in downwind pollution outcomes per 1 SD decrease in upwind forest cover. Each line represents a separate regression using standardized pollutant concentrations as the outcome variable.

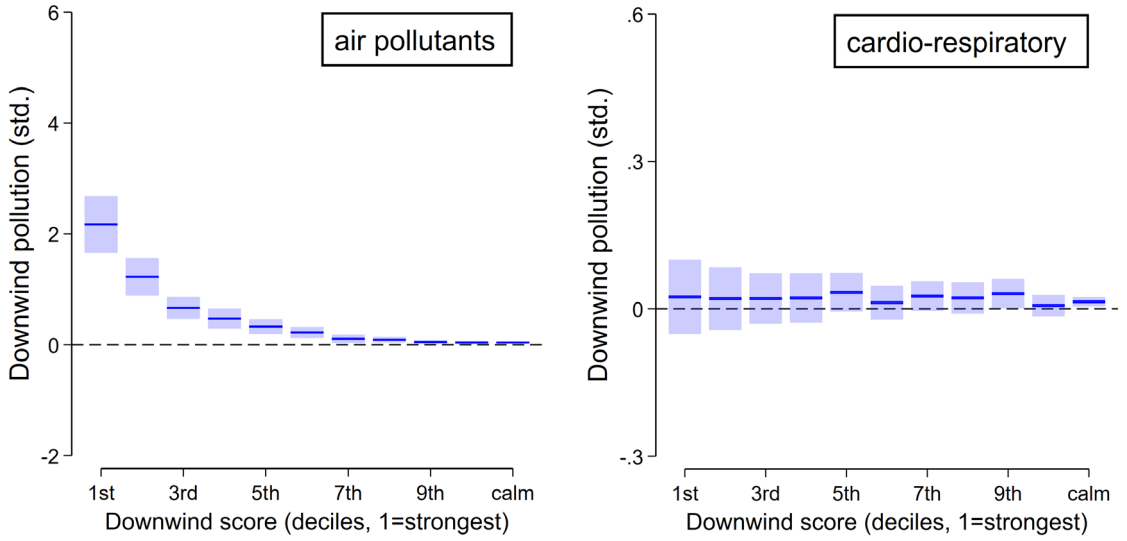
Appendix Figure 9. The Downwind Effect of Forests: Heterogeneity by Prior Land Type



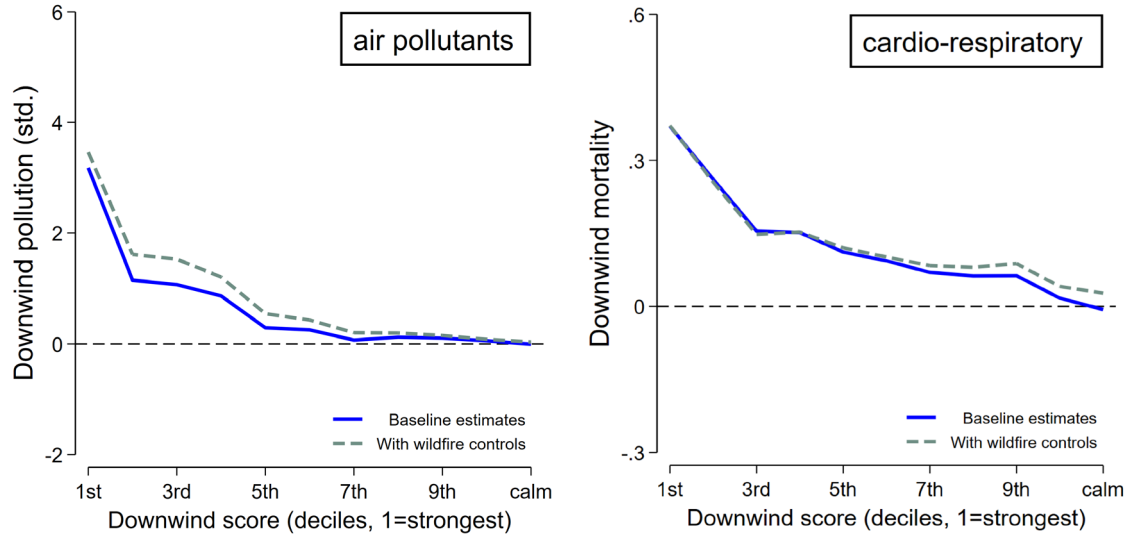
Notes: Charts show estimates on changes in downwind outcomes per 1 SD decrease in upwind forest cover, separately by land cover in the previous year. We use land cover transition information to classify each upwind city-year's forest volume based on its land cover type from the previous year, distinguishing how much of the current year's forest acreage was previously forest, non-forest vegetation land, agricultural land, or non-vegetated land (i.e., urbanized area). We then separately estimate the impacts of upwind forests losses on downwind air quality and cardio-respiratory mortality based on the previous year's land cover.

Appendix Figure 10. The Downwind Effects of Forest Losses: Fire Controls

(a) Direct Fire Effect Estimates



(b) Forest Effect Estimates, with and without Fire Effect Controls



Notes: Panel (a) shows estimates on changes in downwind outcomes per 1 SD increase in fire activities. Panel (b) shows estimates on changes in downwind outcomes per 1 SD increase in upwind forest cover, separately by downwind exposure score bins. Each chart shows two separate regression, one with and the other without controls for upwind fire occurrences.

Appendix Table 1. Major Import Countries Selection

Country	Rank in 2011	Years with missing UN total import data	Years with missing UN import to Brazil and missing Comex export data	Years with low correlation in 2010-2019: UN import to Brazil vs. Comex export (below 0.8)	Mismatch between UN import data HS4 and HS2 (difference>3%, 23y*24 HS2, <27 mismatches)	Selected
USA	1	0	0	0	0	Yes
Germany	2	0	0	0	200	No
Japan	3	0	0	0	0	Yes
China	4	0	0	0	0	Yes
United Kingdom	5	0	0	0	21	Yes
Netherlands	6	0	0	0	11	Yes
France	7	0	0	0	2	Yes
Italy	8	0	0	0	96	No
Belgium	9	2	2	3	0	No
Russian Federation	10	0	0	0	0	Yes
Spain	11	0	0	0	72	No
Canada	12	0	0	0	0	Yes
Rep. of Korea	13	0	0	0	0	Yes
Mexico	14	0	0	2	87	No
China, Hong Kong SAR	15	0	0	0	0	Yes
Nigeria	16	2	2	1	3	No
Saudi Arabia	17	1	1	0	0	No
Poland	18	0	0	0	0	Yes
Indonesia	19	0	0	0	0	Yes
Malaysia	20	0	0	0	0	Yes
Sweden	21	2	0	0	0	No
India	22	0	0	0	8	Yes
Egypt	23	1	0	0	8	No
United Arab Emirates	24	3	23	0	15	No
Denmark	25	0	0	1	17	No
Austria	26	0	0	10	0	No
Switzerland	27	1	0	10	3	No
Singapore	28	0	0	0	53	No
Australia	29	0	0	0	0	Yes
Portugal	30	0	0	0	4	Yes
Brazil	31	0	21	2	0	No
Other Asia, nes	32	0	23	0	12	No
Thailand	33	1	0	0	1	No
Türkiye	34	1	0	0	23	No
Algeria	35	2	2	0	2	No
Iran	36	5	6	4	2	No
Viet Nam	37	3	3	0	0	No
Greece	38	0	0	0	0	Yes
Czechia	39	0	0	10	39	No
Ireland	40	0	0	8	3	No
Bangladesh	41	6	6	0	11	No
Norway	42	0	0	10	1	No
Venezuela	43	6	6	0	8	No
South Africa	44	3	3	0	2	No
Philippines	45	0	0	0	0	Yes
Ukraine	46	1	0	2	4	No
Romania	47	0	0	0	119	No
Finland	48	0	0	0	10	Yes
Morocco	49	0	0	0	6	Yes
Chile	50	0	0	0	0	Yes

Notes: This table tabulates Brazil's major export destinations ranked by Brazil's export value, highlighting countries that are selected in constructing the shift-share instruments. Excluded countries are those with either missing UN import or Comex export data, low correlation between UN import and Comex export data, or those with high numbers of mismatches between UN import HS-4 and HS-2 product categories.

Appendix Table 2. Trade-Deforestation Regression Estimates: Alternative IV Construction

	(1)	(2)	(3)	(4)	(5)	(6)
Panel A. First stage	Export (Δ1y)	Export (Δ2y)	Export (Δ3y)	Export (Δ4y)	Export (Δ5y)	Export (Δ6y)
Shift-share IV	-0.033	0.751***	0.748***	0.411***	0.551***	0.384***
	(0.082)	(0.167)	(0.164)	(0.123)	(0.128)	(0.132)
Panel B. Second stage	Forest (Δ1y)	Forest (Δ2y)	Forest (Δ3y)	Forest (Δ4y)	Forest (Δ5y)	Forest (Δ6y)
ΔExport per capita (1000 BRL)	1.026	-0.084***	-0.128***	-0.275***	-0.202***	-0.269**
	(2.49)	(0.03)	(0.03)	(0.09)	(0.05)	(0.11)
Observations	68,585	68,585	64,814	57,189	49,564	41,939
First-stage F (Kleibergen-Paap)	0.17	20.1	20.8	11.2	18.6	8.5
Year FE	Yes	Yes	Yes	Yes	Yes	Yes
Macroregion FE	Yes	Yes	Yes	Yes	Yes	Yes
Control	Yes	Yes	Yes	Yes	Yes	Yes

Notes: The IVs are constructed based on the agricultural imports by top import countries. All monetary values have been deflated by the Brazilian Consumer Price Index (IPCA) calculated by IBGE and are denominated in 2019 reals. *: $p < 0.10$; **: $p < 0.05$; ***: $p < 0.01$.

Technical Appendix: Area of Effect Estimation Details

This appendix details the construction of a matrix summarizing monthly wind-flow intensities between all pairs of cities in Brazil. We develop an area-of-effect (AoE) model that simulates atmospheric transport from a "sender" city to various "receiver" cities and computes a downwind influence score for each pair. The model traces wind trajectories (streamlines) originating from a given city and day, following the prevailing wind direction and speed on a daily basis. The result is a comprehensive matrix of upwind–downwind linkage intensities for each city pair in each month.

Wind Data and Interpolation. he AoE model uses daily wind direction and speed data for each city (derived from ERA5 reanalysis at 0.25° resolution). As a first step, we generate a continuous wind vector field for each day over Brazil by interpolating the city-level wind data onto a latitude–longitude grid covering the country. We choose the grid's spatial resolution (denoted Δ) to balance accuracy and computational tractability: a finer grid yields more precise wind representations at the cost of longer computation time. In practice, we set Δ such that the grid is sufficiently fine to capture key variations in wind patterns while keeping computation time reasonable (on the order of the country's width divided into a few hundred increments). The daily wind field on this grid allows us to estimate wind vectors at any location in Brazil via interpolation.

Stepwise Trajectory Simulation. Using the wind field, we simulate how wind carries pollutants from each sender city through time. The procedure can be summarized as follows:

1. Initialization: Select a sender city i and a start day d. Set the step index $t = 0$ and initialize the current position p_0 to the coordinates of city i. We also define an initial search radius rad_0 = 300 km (this radius will expand over time, as described below).
2. Iterative wind advection (up to 7 days): For $t = 0,1, \dots ,6$ (a one-week trajectory):
   - Construct the wind vector field for day $d + t$ on the grid, and interpolate to obtain the wind vector at the current position p_t. Denote this interpolated wind vector as w_t, which has direction (bearing) and speed components
   - Identify all potential receiver cities r located within a radius rad_t of the current position p_t. This defines the "downwind footprint" at step t
   - For each such city r, compute a raw downwind intensity score $Wind_{i\to r,d,t}$ that captures the contribution of city i (starting on day d) to city r's pollution on day $d + t$. We model this intensity as an exponential decay function of three factors – (i) the time/dispersion step, (ii) the wind direction alignment, and (iii) distance – following guidance from U.S. EPA (2018) and Phillips et al. (2021). In particular, we write:

$$Wind_{i\to r,d,t} = \exp\{-\alpha \cdot rad_t - \beta \cdot |\theta|_{i\to r,d,t} - \gamma \cdot dist_{i\to r,d,t}\}$$

where α, β, γ are empirically calibrated parameters. In this formulation, rad_t is the search radius at step t (which grows with t, reflecting general dispersion over time); $|\theta|_{i\to r,d,t}$ is a measure of the angular deviation of city r from the exact downwind direction of the wind at p_t (with larger θ meaning r is more off-center from the wind path); and $dist_{i\to r,d,t}$ is the distance from the original sender i to the current position p_t (i.e. the total distance the wind has traveled from the source up to step t). Intuitively, this functional form assigns higher intensity when the receiver is close to the wind trajectory and relatively near the source, and lower intensity as the plume disperses over time, deviates in direction, or travels farther. We impose two cut-offs: if a candidate city r lies outside the radius rad_t or if the angular difference is $\theta_{i\to r,d,t} > 0.4$ radian (approximately 23°), then we set $Wind_{i\to r,d,t} = 0$ (meaning city r is considered too far or not sufficiently downwind at that step to receive any pollution from i). We choose parameter values $\{\alpha, \beta, \gamma\} = \{0.8, 0.49, 0.23\}$. These coefficients are chosen empirically so that the function that attributes wind scores over 7 days is approximately continuous. For that purpose, we used visualisations consisting in heatmaps that simulate the wind scores values not only for cities of interest but for all points of the map for different days and different sender cities. Examples of those heatmaps showing the approximate continuity of the wind score function for the final value of the parameters can be seen on the figure below.

- Whenever $t < 6$, coefficients need to be updated for step $t + 1$. We increase rad_t as described previously by 0.2 to obtain rad_{t+1}. We update $p_t = (x_t, y_t)$ by following the local direction and speed of the wind i.e. using w_t :

$$x_{t+1} = x_t + 24 * 3600 * u_t / dist_m((x_t, y_t), (x_t + 1, y_t))$$

$$y_{t+1} = y_t + 24 * 3600 * v_t / dist_m((x_t, y_t), (x_t + 1, y_t))$$

$$p_{t+1} = (x_{t+1}, y_{t+1})$$

To understand those expressions, we must consider that x and y coordinates are in degrees while the vectors' coordinates u and v are in m/s. The distance (positive or negative) in meters crossed by the wind in 24 hours is of $d_{m,x} = 24 * 3600 * u_t$ along the x-axis and $d_{m,y} = 24 * 3600 * v_t$ along the y-axis. To obtain an approximation of the distance d_p crossed in polar coordinates corresponding to a distance d_m in meters, we use a cross product : if a delta of 1 degree in longitude at the latitude y_t represents $dist_m((x_t, y_t), (x_t + 1, y_t))$ meters, then, an approximation of d_p is $d_p \approx 1 * d_m / dist_m((x_t, y_t), (x_t + 1, y_t))$. Thus,

$$d_{p,x} \approx 1 * d_{m,x} / dist_m\big((x_t, y_t), (x_t + 1, y_t)\big)$$

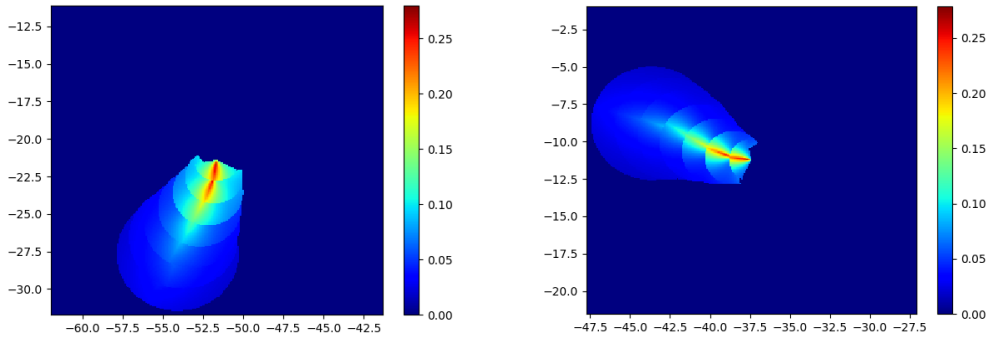
$$d_{p,y} \approx 1 * d_{m,y} / dist_m((x_t, y_t), (x_t + 1, y_t))$$

hence the expression of $x_{t+1} = x_t + d_{p,x}$ and $y_{t+1} = y_t + d_{p,y}$.

We can then proceed to step $t + 1$.

Starting from each particular sender city and day of our sample period, we iterate the procedure for seven steps (i.e., a week) so for $t = 0$ to $t = 6$.

Examples of wind indexes heat maps for two senders



Aggregation to Monthly Intensities. The raw outputs of the AoE simulation are step-level intensity contributions $\text{Wind}_{i\to r,d,t}$ (for $t = 0,1, \dots ,6$) associated with specific sender–receiver–day combinations. We next aggregate these contributions first to the daily level and then to the monthly level for use in our econometric analysis.

We combine step-wise contributions so that each sender–receiver pair (i, r) has a single daily downwind intensity score on each day that reflects all pollution from i arriving in r on that day. If a wind starting in city i on day d reaches city r after t days, we assign that contribution to day $d + t$ for the pair. Formally:

$$\text{Wind}_{i\to r,d'} = \sum_{d+t=d'} \text{Wind}_{i\to r,d,t}$$

To integrate these results into a panel regression framework, we further aggregate the daily indices to the monthly level. This aggregation consists in computing average intensity scores for each tuple (sender city i, receiver city r, month of arrival m):

$$\text{Wind}_{i\to r,m} = \text{Average}_{d'\in m}\ \text{Wind}_{i\to r,d'}$$

This averaging smooths out daily fluctuations and drastically reduces the dimensionality of the data, which makes the regressions computationally manageable. We construct $\text{Wind}_{i\to r,m}$ for all months from January 1997 to December 2019. Because our wind simulations covered 1997–2019, we implicitly assume that each month-of-year's wind pattern is recurrent; in practice, we assign the intensity for, say, January 2010 to be equal to the average intensity we computed for January (across 1997–2019) for the same pair (i, r). If a given pair had no wind connection in a particular month during the study period (i.e. $\text{Wind}_{i\to r,d}$=0 for all days d in that month

window), we record its monthly intensity as 0 (or "calm" conditions as we call it in the paper) for that month in all years. The final output is a matrix of monthly intensity scores $\text{Wind}_{i \to r,m}$. This upwind–downwind intensity matrix forms the basis for our downstream pollution and health impact analysis in the paper.